3D-Bioprinted Mini-Brain: A Glioblastoma Model to Study cellular interactions and therapeutics

Marcel Alexander Heinrich, Ruchi Bansal, Twan Lammers, Yu Shrike Zhang, Raymond Schiffelers, Jai Prakash**

M.A. Heinrich, Dr. R. Bansal, Prof. T. Lammers, Prof. J. Prakash

Department of Biomaterials Science and Technology, Targeted Therapeutics Section, Technical Medical Centre, University of Twente, Enschede, The Netherlands

Email of corresponding authors: j.prakash@utwente.nl and m.a.heinrich@outlook.com

Prof. T. Lammers

Department of Nanomedicine and Theranostics, Institute for Experimental Molecular Imaging, RWTH Aachen University Clinic, Aachen, Germany

Dr. Y.S. Zhang

Division of Engineering in Medicine, Department of Medicine, Harvard Medical School, Brigham and Women's Hospital, Cambridge, MA, USA

Prof. R. Schiffelers

Department of Clinical Chemistry and Hematology, University Medical Center Utrecht, Utrecht, The Netherlands

Keywords: 3D Bioprinting, Glioblastoma microenvironment, Drug Screening, Tumor-associated macrophages, Mini-Brain

Abstract

Glioblastoma-associated macrophages (GAMs) play a crucial role in the progression and invasiveness of glioblastoma multiforme (GBM); however, the exact crosstalk between GAMs and glioblastoma cells is not fully understood. Furthermore, there is a lack of relevant in vitro models to mimic their interactions. Here, novel 3D-bioprinted mini-brains consisting of glioblastoma cells and macrophages are presented as tool to study the interactions between these two cell types and to test therapeutics that target this interaction. It is demonstrated that in the mini-brains, glioblastoma cells actively recruit macrophages and polarize them into a GAM-specific phenotype, showing clinical relevance to transcriptomic and patient survival data. Furthermore, it is shown that macrophages induce glioblastoma cell progression and invasiveness in the mini-brains. Finally, it is demonstrated how therapeutics can inhibit the interaction between GAMs and tumor cells resulting in reduced tumor growth and more sensitivity to chemotherapy. It is envisioned that this 3D-bioprinted tumor model is used to improve the understanding of tumor biology and for evaluating novel cancer therapeutics.

Main Text

Within the tumor microenvironment (TME), dynamic crosstalk between cancer cells and other cells drive tumor growth and metastasis.[1] In glioblastoma multiforme (GBM), macrophages are one of the most important and abundant cell types recruited and polarized by cancer cells towards glioblastoma-associated macrophages (GAMs), which support tumor progression, invasion and angiogenesis.[2-4] Studies have shown that intervening into the interaction between cancer cells and macrophage can retard GBM progression, as shown in preclinical models.[5, 6] *In vivo* models are arguably the closest to the human disease, but lack simplicity to accurately determine the interactions between specific cell types due to the influence from other TME components. Therefore, there is an urgent need for suitable *in vitro* models that properly recapitulate the biologically relevant interactions between macrophages and glioblastoma cells in GBM and act as a platform to test newly developed drugs.

In recent years, 3D *in vitro* models have been increasingly brought into focus due to their capacities to mimic tissue-like feature and cellular interactions found in the TME.[7, 8] Earlier we have developed 3D hetero-spheroid models to mimic the fibrotic environment, which displayed stromal cell-specific characteristics and successfully applied for studying nanomedicine.[9] A different approach was followed by Kilian *et al*, who developed a method to rapidly extrude alginate fibers encapsulating breast tumor cells and macrophages to investigate breast cancer metastasis.[10] However, most of these models are limited with regard to cell numbers or only focus on one characteristic of the *in vivo* situation. Furthermore, the inclusion of certain cell types in such models is limited.

Recent advancements in the 3D bioprinting technologies have facilitated the construction of clinically relevant biomimetic tissues, which are able to replicate the delicate architecture and complex composition of different tissues and applied for the tissue regeneration.[11, 12] Such models will allow to test drugs in a realistic environment before

embarking on animal studies, eventually contributing to reducing and refining animal experiments. Due to this versatility, 3D bioprinting can be a promising tool to create 3D models that mimic the architecture and cellular composition of GBM, allowing us to better study the tumor biology as well as screen drugs in a relevant environment.

In this study, we demonstrate the feasibility of creating a miniaturized brain (called here "mini-brain") to the lab scale in the form of 3D bioprinted model. The mini-brain can be created with mesoscale dimensions and cultured under conventional cell culture conditions. Although this model is not representing stem cell originated real tissue, combination of different cells using 3D bioprinted approach will certainly allow cells to re-organize and interact with each other. One may use 3D bioprinting to print different cells in specific pre-arranged structure to provide more features of an original tissue. To demonstrate that the current model recapitulates the interaction between cancer cells and macrophages, we incorporated a well-defined mass of tumor cells into the mini-brain comprised of macrophages and studied phenotypic alterations in both macrophages and cancer cells resulting from this close interaction. Finally, we demonstrated that this model can be used for examining the therapeutic efficacy of conventional chemotherapy as well as macrophage modulating drugs. The proposed technology is likely to advance the field of 3D *in vitro* models by offering relevant biomimetic characteristics and processes, which are not achievable with other culture systems. Most of all, our novel 3D-bioprinted *in vitro* model is not only limited to mimic GBM, but may be translated to different types of cancer and diseases.

The strategy we present is based on a two-step bioprinting process in which we first print the larger brain model encapsulating a mouse macrophages cell line (RAW264.7) with an empty cavity, which in the second step is filled with mouse glioblastoma cells (GL261) embedded into bioink, followed by photo-crosslinking of the construct (**Figure 1A**). We encapsulated these cells into a blend bioink consisting of 3% w/v gelatin methacryloyl (GelMA, at high degree of methacrylation (**Supplementary**

Figure S1)) and 4% w/v gelatin, selected based on optimized concentrations (**Supplementary Figures S2**). Previously,

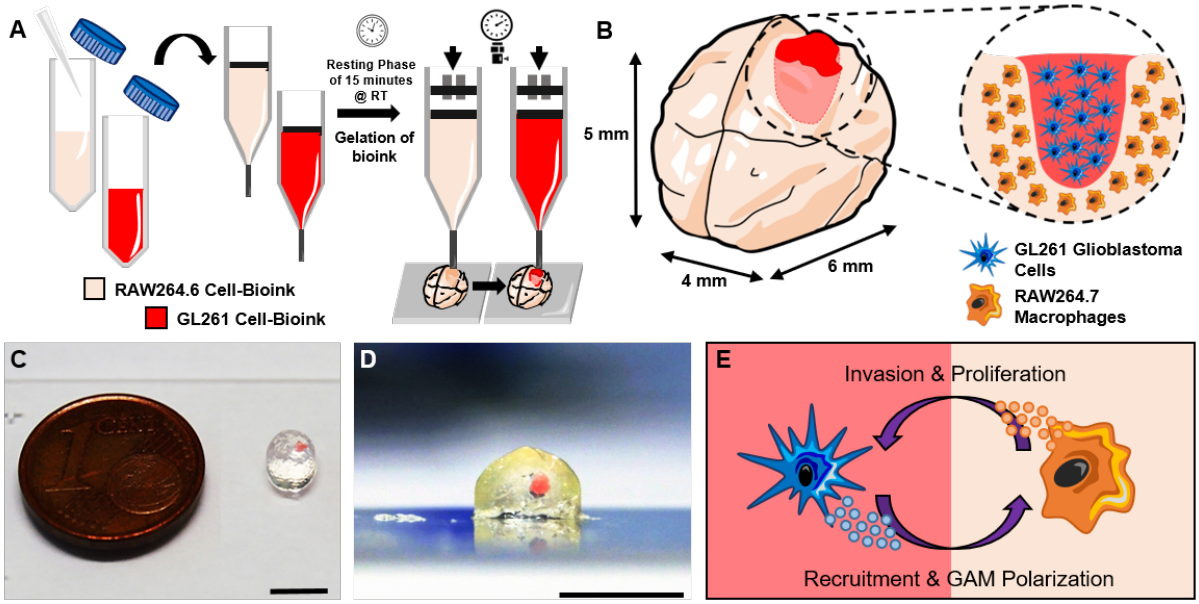

Figure 1 Schematic representation of the bioprinting process and the bioprinted mini-brains. A) Bioprinting process displaying the preparation of the cell-laden GelMA-gelatin bioinks and further 2 step bioprinting of the mini-brains. B) Close up and cross-sectional view of the cell-laden bioprinted mini-brains. C) Bioprinted mini-brains highlighting the glioblastoma area in red, scale bar = 5 mm. D) Cross-section in the frontal plain of the bioprinted mini-brains with highlighted glioblastoma area in red, scale bar = 5 mm. E) Schematic of the crosstalk between glioblastoma cells and macrophages.

GelMA has proven optimal performance in bioprinting applications due to its biocompatibility and shear-thinning properties.[13, 14] Gelatin on the other hand gives stability to the construct immediately after extrusion. Additional water-loss at 37°C results in pores with large diameters. In this way, we could fabricate 3D-bioprinted mini-brains consisting of both cell types, where the location of the tumor area was well-defined, which should enable crosstalk similar to the *in vivo* situation (**Figure 1B-1E**).

First, we demonstrated that the developed bioink could successfully encapsulate cells after being extruded as part of the bioprinting process and retain a stable 3D shape. To characterize the mechanical properties of the bioink, we investigated the storage (G') and loss (G'') moduli as well as the complex viscosity (η*). First, we found that the bioink was stable over time based on the nearly constant values for G', G'' and η* (**Supplementary Figure S3A & S3B**). Furthermore, we observed that the bioink at 37 °C behaved like a liquid with a non-detectable G', low G'' and low η*, enabling simple mixing of cells and bioink. Whereas the bioink at 20 °C displayed high values for G', G'' and η*, indicating the full gelation of the bioink at RT and therefore conditions of printing. In particular, we detected a G' of 1000 Pa and storage modulus between 10-20 Pa at the conditions of printing, which we previously demonstrated to be optimal parameters to be used in 3D bioprinting applications.[14] We next investigated the rheological properties in relation to an increasing shear rate at 20 °C. Here we observed that with increasing shear rate, G' and G'' remained relatively stable, indicating sufficient stability of the bioink for bioprinting (**Supplementary Figure S3C**). More importantly, we observed that η* rapidly decreased with increasing shear rate, confirming the shear-thinning properties of our bioink (**Supplementary Figure S3D**), which have shown to be optimal for bioprinting applications.[14] When then investigated the average pore size of the crosslinked gel after allowing gelatin to leak out of the construct, which was measured to be 17.08 ± 6.7 μm as based on scanning electron microscopy which is suitable for cells to freely migrate and move through the construct (**Supplementary Figure S3E & S3F**). As the bioink displayed promising characteristics to be functional for bioprinting cell-laden constructs, we further investigated the influence of bioprinting on the chosen cell lines. RAW264.7 macrophages and GL261 glioblastoma cells were separately mixed with the bioink at 37°C to ensure simple and homogenous mixing and transferred to a syringe, followed by a resting period of 15 min at room temperature to ensure gelation of the bioink. Using a custom-

modified bioprinter, we bioprinted cell-laden mini-brains as described above containing either RAW264.7 or GL261 cells. The cell viability was determined post-bioprinting on day 0, 4 and 10 and we found that both, RAW264.7 and GL261 cells, remained viable over the total duration of the experiment (**Supplementary Figure S4A & S4B**). Additionally, the cell-laden constructs displayed high metabolic activity measured on days 1, 4, 7 and 10 post-bioprinting **(Supplementary Figure S4C & S4D**).

To investigate the crosstalk between tumor cells and macrophages, we set up to different models to study (i) the paracrine and (ii) the juxtacrine signaling between these cells. In the paracrine model, we first bioprinted mini-brains containing either GL261 or RAW264.7 cells and cultured them together in the same well ensuring interaction solely via secreted cytokines and growth factors (**Figure 2A**). After 4 days, we separated the mini-brains and investigated the expression profiles of genes, which have been reported to play a major role in GBM (see **Supplementary Table S1** for abbreviations of genes not described in the text, and **Supplementary Tables S2 and S3** for detailed gene sequences used).[2, 3, 15] Remarkably, we first found that compared to conventional 2D culture, macrophages in our model had enhanced expressions of ECM-remodeling enzymes (matrix metallopeptidases 2 (Mmp2) and 9 (Mmp9)), GAM phenotypic markers (fibroblast growth factor 2 (Fgf2), interleukin 1β (Il-1β), arginase 1 (Arg-1), and other crucial genes shown to be overexpressed by GAMs *in vivo* (**Supplementary Figure S5A**).[2] Interestingly, we found that GBM-specific markers Gfap and chitinase like 1 (Chil1), which are highly expressed *in vivo*, showed upregulation of up to 15-fold in the GL261 cells in our 3D model when compared to the 2D monolayer culture (**Supplementary Figure S5B**). Additionally, we observed a 100-fold overexpression of C-C motif chemokine ligand 2 (Ccl2), a chemoattractant, which may account for the enhanced GAM recruitment capacity of these cells.[16] We also overserved a significant increase in the expression of glycoprotein NMB (Gpnmb) in glioblastoma cells, whereas this marker is

significantly downregulated in macrophages, displaying how different cell types react differently in the 3D environment. These data are line of other studies which showed that 3D microenvironment provides low stiffness, high cell-to-cell contact in 3D space (shown with SEM images), and improves autocrinal activation, compared to 2D culture on stiff plastic.[7, 17] Interestingly, co-culturing of glioblastoma mini-brains with macrophage mini-brains, allowing crosstalk with an exchange of secreted cytokines and growth factors in a paracrine manner, further positively activated both cell types in the context of GBM. We found that GAM-specific markers (Fgf2, Arg-1, Il-1β, mannose receptor C-type 1 (Mrc1), and secreted phosphoprotein 1 (Spp1)) were highly expressed in the RAW264.7 mini-brain co-cultured in the presence of GL261 mini-brain, compared to the RAW264.7 mini-brain without co-culture (**Figure 2B** & **Supplementary Figure S6A**). Furthermore, we also found a significant upregulation of glioblastoma markers in the GL261 mini-brains, when cultured in the presence of RAW264.7 mini-brains, compared to the GL261 mini-brains cultured without macrophages (**Figure 2C** & **Supplementary Figure S6B**). In particular, the gene expression of markers involved in macrophage recruitment (Ccl2) and polarization (Spp1), GBM markers (Gfap, Chil1) and matrix remodeling (Mmp2, Mmp9) were significantly induced.

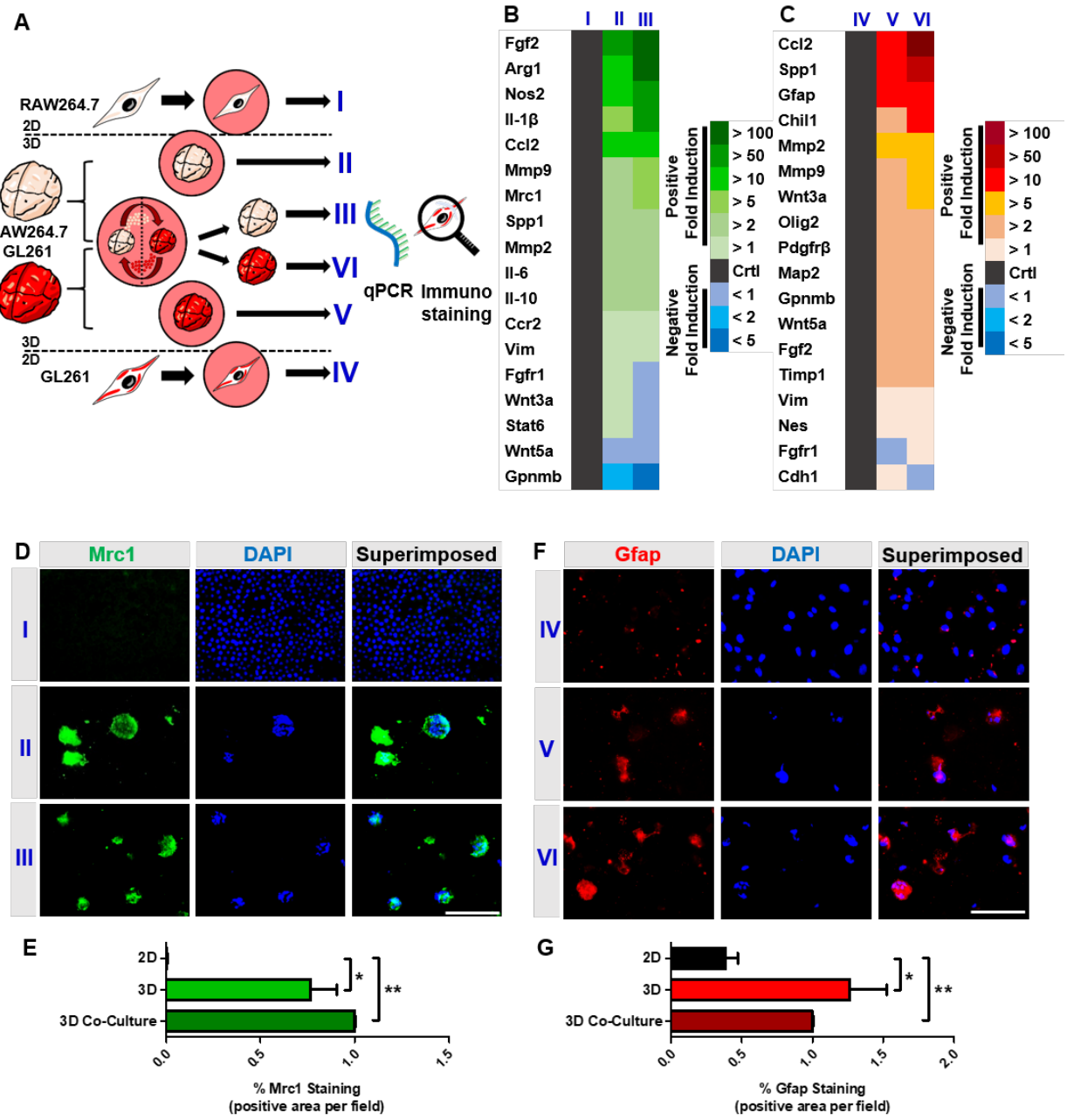

Figure 2 Paracrine signaling between separately bioprinted RAW264.7 and GL261 cell-laden mini-brains in co-culture. A) Schematic representation of the experimental setup for separately bioprinted RAW264.7 and GL261 in co-culture. B) Heat map of expressed genes in RAW264.7 macrophages for (I) 2D monolayer, (II) 3D single bioprinted and (III) 3D separately bioprinted co-culture with GL261. C) Heat map of expressed genes in GL261 glioblastoma cells for (IV) 2D monolayer, (V) 3D single bioprinted and (VI) 3D separately bioprinted co-culture with RAW264.7. D, E) Immunofluorescent staining for (D) Mrc1 (green

(pseudo-color)) and DAPI (blue) in RAW264.7 macrophages for 2D monolayer, 3D bioprinted and 3D separately bioprinted co-culture with GL261 and (E) respective quantifications, scale bar = 100 µm. F, G) Immunofluorescent staining for (F) Gfap (red) and DAPI (blue) in GL261 glioblastoma cells for 2D monolayer, 3D bioprinted and 3D separately bioprinted co-culture with RAW264.7 and (G) respective quantifications, scale bar = 100 µm. Data represent mean ± SEM for at least 3 independent experiments. Statistical analysis was performed by two-tailed unpaired student's t-test. *$p < 0.05$, **$p < 0.01$.

To further confirm the upregulation of *in vivo*-specific markers in our novel 3D mini-brains, we studied the protein expressions of Mrc1 and Gfap, as these are the most common markers for GAMs and glioblastoma cells, respectively.[18] With immunofluorescent staining 4 days post-bioprinting, we found that both Mrc1 and Gfap were significantly upregulated in the 3D culture compared to the 2D monolayer, in which these markers were hardly detectable (**Figure 2D – 2G**). With these data, we confirmed that our 3D mini-brains could recapitulate phenotypic characteristics of cells found in GBM *in vivo* and are superior to conventional 2D culture. Yet, within the TME besides exchanging cytokines different cell types also have direct cell-to-cell contact in a juxtacrine manner and thereby activate each other via different membrane receptors and ligands eventually controlling cell phenotypes such as migration.[19] [20]

In the juxtacrine bioprinted model, we studied the migration and crosstalk between RAW264.7 and GL261 when they have the ability to engage in direct cell-to-cell contact. As Cell migration is mainly facilitated by the capability of cells to attach to the provided surface,[21] we first investigated the attachment of our cells onto the bioink matrix in comparison to conventional culture well plate. Both RAW264.7 and GL261 cells attached to the bioink matrix as confirmed by immunofluorescent staining against F-actin/ DAPI and

scanning electron microscopy for RAW264.7 (**Figure 3A – 3C**) and GL261 (**Figure 3D – 3F**), respectively. To study the migration behavior of these cells, we developed a custom-designed migration assay by placing bioprinted mini-brains with either RAW264.7 macrophages or GL261 cells, on top of a monolayer of the opposite cells (**Supplementary Figure S7**). After 4 days of culture, we found that RAW264.7 macrophages fully grown inside the mini-brains. After 24 h of direct contact, macrophages significantly migrated towards GL261 cells in large numbers compared to migration towards empty wells or themselves (**Figure 3G & 3H**), indicating glioblastoma cells actively recruited the macrophages. In the other case, GL261 mini-brains, cultured for 10 days, were placed on monolayers of either tumor cells or macrophages. Although tumor cells were less migratory, they showed a significantly higher migration towards RAW264.7 macrophages compared to empty wells or themselves (**Figure 3I & 3J**). These data demonstrate that tumor cells are able to attract macrophages to their site and educate them to support their own survival and growth. To further investigate the effects of direct crosstalk between the cells in our mini-brains at transcriptome level, we bioprinted mini-brains consisting of RAW264.7 macrophages including a cavity filled with GL261 cells, mimicking a realistic microenvironment. After 4 days of culturing, we resected the glioblastoma area and analyzed the effects of the direct crosstalk between these two cells (**Figure 3K & Supplementary Figure S8**). When macrophages were cultured in direct cell-to-cell contact with glioblastoma cells, we found that GAM-specific markers (Fgf2, Il-1β, Arg-1, Nos2, fibroblast growth factor receptor 1 (Fgfr1)), interleukins 10 (Il-10) and 6 (Il-6)) and markers for matrix remodeling (Mmp2, Mmp9) were highly overexpressed when compared to mini-brains in 3D monoculture (**Figure 3L & Supplementary Figure S9A**). Furthermore, GL261 cells showed very high expression levels of specific glioblastoma markers (Gfap, Chil1, oligodendrocyte transcription factor 2 (Olig2), platelet-derived growth factor receptor β (Pdgfrβ), tissue inhibitor of

metallopeptidase 1 (Timp1) as well as a 500-fold induction of Spp1 (**Figure 3M & Supplementary Figure S9B**).

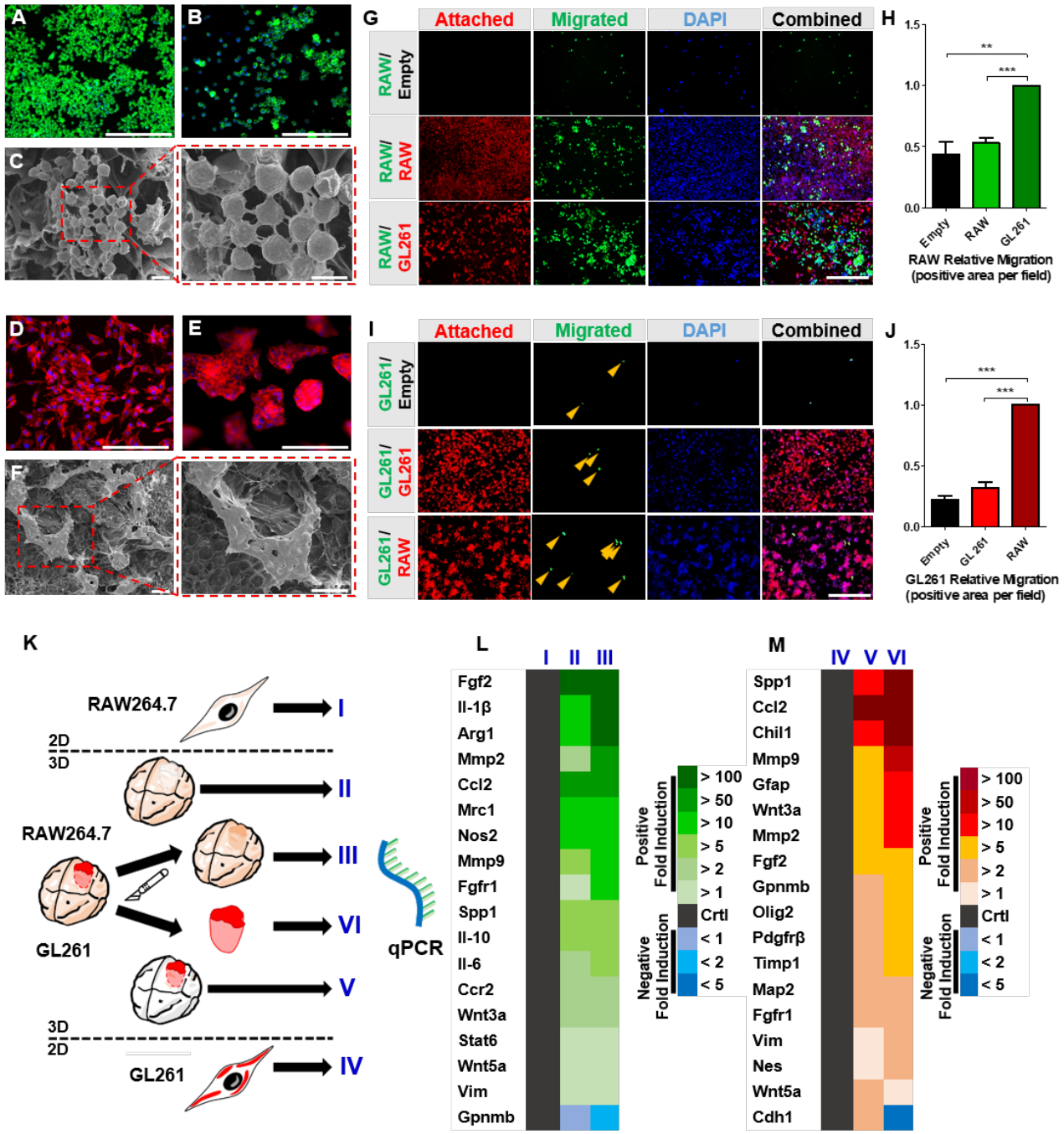

Figure 3 Migration and juxtacrine signaling between RAW264.7/GL261 cell-laden mini-brains in direct cell-to-cell contact. A) RAW264.7 macrophages stained for f-actin (green (pseudo-color)/ nuclei (blue) (A) in well plate and (B) on top of crosslinked construct, scale bar = 200 µm. C) SEM image for attached RAW264.7 macrophages, scale bar = 10 µm. D, E)

Attached GL261 glioblastoma cells stained for f-actin (red)/ nuclei (blue) (D) in well plate and (E) on top of crosslinked construct, scale bar = 200 µm. F) SEM image for attached GL261 glioblastoma cells, scale bar = 50 µm. G, H) Migration assay for green CMFDA-labelled RAW264.7 towards empty (top), orange CMRA-labelled RAW264.7 (middle) and CMRA-labelled GL261 (bottom) after 4 days of culture in the gel and (H) respective quantifications. I, J) Migration assay for green CMFDA-labelled GL261 towards empty (top), orange CMRA-labelled GL261 (middle) and CMRA-labelled RAW264.7 (bottom) after 10 days of culture in the gel and (J) respective quantification (migrated cells indicated by orange arrows). K) Schematic of the experimental set-up for bioprinted RAW264.7/GL261 co-culture model. L) Heat map of expressed genes in RAW264.7 macrophages for (I) 2D monolayer, (II) 3D single bioprinted and (III) 3D bioprinted RAW264.7/GL261 co-culture model. M) Heat map of expressed genes in GL261 glioblastoma cells for (IV) 2D monolayer, (V) 3D single bioprinted and (VI) 3D bioprinted RAW264.7/GL261 co-culture model Data represent mean ± SEM for at least 3 independent experiments. Statistical analysis was performed by two-tailed unpaired student's t-test.**$p < 0.01$, ***$p < 0.001$.

Furthermore, our mini-brains also displayed characteristics of epithelial-to-mesenchymal transition of glioblastoma cells such as an increased expression of vimentin (Vim) and nestin (Nes) as well as a significant loss of e-cadherin (Cdh1), which indicated that glioblastoma cells attained a migratory phenotype. Both findings are consistent with the performed migration assay where cells displayed low but present migration behavior when cultured with RAW264.7 macrophages. The findings in the juxtacrine model combining both cell types in a single mini-brain displayed the potential of our model to be of significant clinical relevance and resemble the characteristics found *in vivo* to a great extent.

To confirm that the genes upregulated in our mini-brains are of clinical relevance, we performed a transcriptomic analysis of publicly available data. Data from 159 GBM patients

versus 8 control patients were analyzed to know the significance of the most upregulated genes in macrophages (Fgf2, Il-1β, Arg1, Mmp2) and glioblastoma cells (Spp1, Ccl2, Chil1, Mmp9) in our mini-brains and of the most downregulated genes in either of these cells

(Gpnmb, Cdh1).

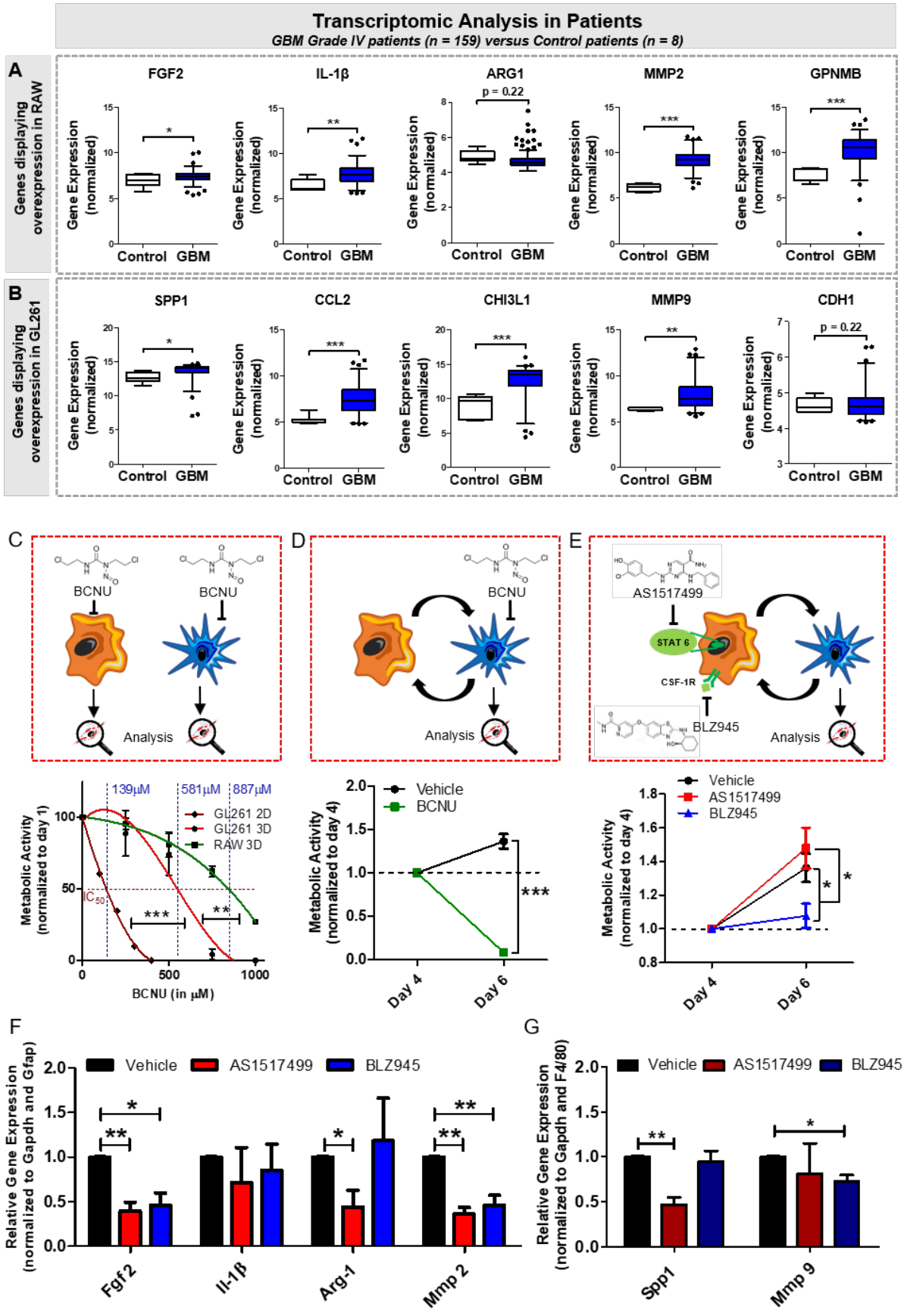
Transcriptomic Analysis in Patients
GBM Grade IV patients (n = 159) versus Control patients (n = 8)
A
Genes displaying overexpression in RAW
FGF2
IL-1β
ARG1
p = 0.22
MMP2
GPNMB
Gene Expression (normalized)
Control GBM
B
Genes displaying overexpression in GL261
SPP1
CCL2
CHI3L1
MMP9
CDH1
p = 0.22
C
BCNU
Analysis
D
BCNU
Analysis
E
AS1517499
STAT 6
CSF-1R
BLZ945
Analysis
139μM
581μM
887μM
GL261 2D
GL261 3D
RAW 3D
IC50
Metabolic Activity (normalized to day 1)
BCNU (in μM)
Vehicle
BCNU
Metabolic Activity (normalized to day 4)
Day 4
Day 6
Vehicle
AS1517499
BLZ945
F
Relative Gene Expression (normalized to Gapdh and Gfap)
Fgf2
Il-1β
Arg-1
Mmp 2
G
Relative Gene Expression (normalized to Gapdh and F4/80)
Spp1
Mmp 9

Figure 4 Comparative transcriptomic analysis in human GBM patients and performance of immuno- and chemotherapeutic drug compounds in the bioprinted mini-brains A, B) Transcriptomic analysis in human cohort from public database GEO (GSE16011) for genes found to be upregulated in the 3D bioprinted mini-brains (A) primarily for RAW264.7 macrophages and (B) primarily for GL261 glioblastoma cells. C) (Top) Schematic representation of the treatment with BCNU in mini-brains containing either RAW264.7 or GL261 in monoculture and (bottom) concentration dependent metabolic activity and highlighted IC_{50} of GL261 cells in 2D monolayer and GL261 and RAW264.7 3D monocultures 4 days post-bioprinting after treatment with BCNU in different concentration for 48h. D) (Top) Schematic representation of treatment with BCNU in the cocultured RAW264.7/GL261 mini-brains and (bottom) metabolic activity of GL261 after co-culture with RAW264.7 for 4 days and treatment with vehicle or BCNU for 48h after separation of the two cell types on day 4. E) (Top) Schematic representation of treatment with either AS1517499 or BLZ945 in the cocultured RAW264.7/GL261 mini-brains and (bottom) metabolic activity of GL261 after co-culture with RAW264.7 for 4 days and treatment with vehicle, AS1517499 or BLZ945 on day 1 and 3 post-bioprinting and separation of the two cell types on day 4 (the same vehicle group was used in experimental setups (D) and (E)). (F) Gene expression for selected genes in RAW264.7 after 4 days of culture and after treatment with either AS1517499 or BLZ945 on day 1 and 3 post-bioprinting. (G) Gene expression for selected genes in GL261 after 4 days of culture and after treatment with AS1517499 or BLZ945 on day 1 and 3 post-bioprinting. Data represent mean ± SEM for at least 3 independent experiments. Statistical analysis for experiments comparing 2 groups was performed by two-tailed unpaired student's t-test and two-way ANOVA for multiple treatment groups . *$p < 0.05$, **$p < 0.01$, ***$p < 0.001$.

Intriguingly, we found that the macrophage-specific markers FGF2, IL-1β and MMP2 are significantly overexpressed in GBM patients compared to the control groups (**Figure 4A**). However, ARG1 did not show any upregulation in the GBM patients indicating that this marker might be influenced by other TME components. Furthermore, the glioblastoma cell-specific markers SPP1, CCL2, CHI3L1 (human equivalent to mouse Chil1) and MMP9, found overexpressed in our model, displayed a significant overexpression in GBM patients proving the importance of these markers and clinical relevance of our model (**Figure 4B**). Interestingly, we also found that GPNMB, which is downregulated in macrophages in our model, is highly expressed in GBM patients. However, there was a strong overexpression of GPNMB in glioblastoma cells in our mini-brains, which will altogether result into to an overexpression, as found in GBM patients. On the contrary, CDH1, which is significantly downregulated in glioblastoma cells in our model, does not show any significant difference in GBM patients indicating that other factors might influence the overall expression of this gene in patients, as a low CDH1 expression is characteristic for GBM as described elsewhere.[12, 22]. The different expression of ARG1 and CDH1 in our model might display the limitations of our model but might also indicate that these characteristics are dependent on other components of the TME.[12, 22] By implementing other cell types in our model, for instance glioma-associated astrocytes, which so far have not been fully investigated for their contribution to GBM,[23] and by gradually increasing the complexity of this model, it might be possible to clearly and specifically define the function and contribution from each TME component. To further confirm the clinical significance of the aforementioned genes, we analyzed the survival of 577 GBM patients. Intriguingly we found that high expression of FGF2 showed a poor survival of GBM patients (**Supplementary Figure S10A**). Likewise, high expression of IL-1β also showed a similar trend. Interestingly, GPNMB also displayed significant influence on patient survival, which based on our model can be directly ascribed to

high expression in glioblastoma cells. Moreover, high expression levels of upregulated genes in our mini-brain model such as SPP1, CCL2 and CHI3L1 were found to be clearly correlated with poor survival of GBM patients (**Supplementary Figure S10B**). These correlations demonstrate that the expression of genes in our mini-brains is of profound clinical relevance. In particular, markers that are directly linked to poor patient survival are prominent in our mini-brains.

Lastly, we demonstrated the suitability of this model to be used for the screening of different types of drugs by testing carmustine (BCNU), a common chemotherapy for GBM, and two immunomodulatory drugs, AS1517499, a Stat6 inhibitor, and BLZ945, an inhibitor of colony stimulating factor 1 receptor (Csf-1r) (**Figure 4C – 4G**). We set up three sets of experiments to study the effect on cell growth. In the first experiment, we investigated the effect of BCNU on mono-cultured mini-brains of either macrophages or tumor cells treated from day 4 to day 6 and performed metabolic activity assay (alamar blue assay). We found that the half maximal inhibitory concentration (IC_{50}) of 3D mono-cultured GL261 cells was 581 μM, which was significantly higher compared to the IC_{50} of a conventional 2D cell culture (139 μM) (**Figure 4C**). The higher IC_{50} in 3D culture might be related to the poor diffusion due to high cell-to-cell interactions compared to 2D cultures in which cells are only attached to the plate from one side. RAW264.7 showed high resistance to the treatment (IC_{50} 887 μM). In the second experiment, we examined the effect of BCNU on tumor cells in co-culture. Tumor cells and macrophages were co-cultured in mini-brains for 4 days, and then tumor pieces were isolated and treated with BCNU until day 6 followed by metabolic activity assay. Tumors isolated from the co-cultured mini-brain for 4 days showed significantly higher growth rate compared to the one isolated from the mono-cultured mini-brain. Importantly, BCNU strongly inhibited the growth of tumors isolated from the co-cultured mini-brain than mono-cultured mini-brain (**Figure 4D**). It is established that chemotherapy works more efficiently in rapidly growing

cells[24] and co-culture with macrophages significantly enhanced the tumor cell growth, which can significantly inhibited by chemotherapy. In the third experimental set, we evaluated the effect of immunomodulatory agents Csf-1 inhibitor BLZ945 studied in GBM by Quail *et al*[5] and Stat6 inhibitor AS1517499, previously studied by us for inhibiting M2 macrophage phenotype in breast cancer,[25] in co-culture (**Figure 4E**). We treated co-cultured mini-brain on day 1 and 3 with AS1517499 or BLZ945, isolated tumor pieces and cultured them until day 6 followed by metabolic activity assay. We found that tumors isolated from co-cultured mini-brains treated with BLZ945, but not with AS1517499 showed a slow growth compared to vehicle-treated tumors. These data are in line of the studies by Quail *et al.* in which they showed a direct the effects of BLZ945 on GBM growth *in vivo*[5]. The direct effect of AS1517499 in GBM models remains to be reported in literature and therefore we cannot compare our data. To additionally demonstrate that these drugs indeed inhibit macrophage phenotypes, we examined the gene expression of GBM markers for macrophages and tumor cells. Interestingly, we found that AS1517499 significantly downregulated the gene expression of Fgf2, Arg-1 and Mmp2 in macrophages while BLZ945 only Fgf2 and Mmp2 in the co-cultured mini-brains (**Figure 4F**). Furthermore, we found that the expression of Spp1 and Mmp9 are significantly downregulated in GL261 cells after treatment with AS1517499 and BLZ945, respectively (**Figure 4G**). BLZ945 and other CSF-1R inhibitors are reported to reduce the expression of factors controlling vascularization and ECM-remodeling,[26] which is in agreement with the observed gene expression profiles. These results clearly suggest that the crosstalk between GAMs and tumor cells in GBM has significant effect on tumor growth, which goes well in line with reported literature, and that inhibition of GAMs can result in the reduction of this growth, demonstrating how our model can be used to investigate the effects of therapeutics on these specific interactions.

To our best knowledge, this is the first proof-of-concept bioprinted model of the tumor microenvironment that displays macrophage recruitment and polarization as well as glioblastoma progression and invasion in a single construct, which proves the suitability for bioprinted tumor models to replicate the clinical situation and help in understanding complex interactions in the TME. Furthermore, this is the first bioprinted model that can be used to specifically investigate the effects of immunomodulatory and chemotherapy in a rapid and easy manner, which might eventually facilitate the fabrication of tailored drugs and treatment strategies. By creating different geometries, one can study different aspects as done here for studying cell to cell interaction such as migration and invasion. One may include different cell patterns and structure within a bioprinted tissue to provide specific cell organization. In general, this proof-of-concept study enables the way to more complex models with specifically defined architecture which are only possible using bioprinting. Furthermore, we envision that this model might also find broad application in the testing of such novel treatment strategies and drugs as described above, which would eventually help to reduce and refine animal experiments. Moreover, this model is not solely limited to mimicking the interactions in the glioblastoma microenvironment but might be translated to other types of cancer emulating their unique tumor microenvironments. Altogether, the realistic biomimetic characteristics and behavior of our 3D-bioprinted mini-brains has paved a new avenue for the versatile fabrication of biologically relevant *in vitro* models, where the future bioprinting of complex multicellular TME mimics for rapid drug screening is envisioned.

Supporting Information

Online methods and supporting information are available from the Wiley Online Library or from the author.

Author Contributions

M.A.H. and J.P. conceived the study, designed experiments and co-wrote the manuscript. M.A.H. performed the experiments. R.B. performed the transcriptomic analysis in GBM patients. T.L., R.M.S. and Y.S.Z. provided support and guidance on the study. All authors reviewed the manuscript. Correspondence and requests for materials should be addressed to J.P. and M.A.H.

Competing Financial Interests

The authors declare no conflict of interest.

Acknowledgements

The authors acknowledge funding from the Dutch Technical Foundation and the Dutch Cancer Foundation (STW/KWF; project n. 15204).

Received:

Revised:

Published Online:

References

[1] a) D. Quail, J. Joyce, *Nat. Med.* **2014**, 19, 1423; M. Pickup, S. Novitskiy, H. Moses, *Nat. Rev. Cancer* **2013**, 13, 788; b) M. Binnewies, E. Roberts, K. Kersten, V. Chan, D. Fearon, M. Merad, L. Coussens, D. Gabrilovich, S. Ostrand-Rosenberg, C. Hedrick, R. Vonderheide, M. Pittet, R. Jain, W. Zou, T. Howcroft, E. Woodhouse, R. Weinberg, M. Krummel, *Nat. Med.* **2018**, 24, 541.

[2] S. Roesch, C. Rapp, S. Dettling, C. Herold-Mende, *Int. J. Mol. Sci.* **2018**, 19, 436.

[3] A. Mantovani, F. Marchesi, A. Malesci, L. Laghi, P. Allavena, *Nat. Rev. Clin. Oncol.* **2017**, 14, 399.

[4] P. Allavena, A. Sica, C. Garlanda, A. Mantovani, *Immunol Rev.* **2008**, 222, 161.

[5] D. Quail, R. Bowman, L. Akkari, M. Quick, A. Schuhmacher, J. Huse, E. Holland, J. Sutton, J. Joyce, *Science* **2016**, 352, 6288.

[6] a) D. Yan, J. Kowal, L. Akkari, A. Schuhmacher, J. Huse, B. West, J. Joyce, *Oncogene* **2017**, 36, 6049; b) S. Pyonteck, L. Akkari, A. Schuhmacher, R. Bowman, L. Sevenich, D. Quail, O. Olson, M. Quick, J. Huse, V. Teijeiro, M. Setty, C. Leslie, Y. Oei, A. Pedraza, J. Zhang, C. Brennan, J. Sutton, E. Holland, D. Daniel, J. Joyce, *Nat Med.* **2013**, 19, 1264; c) P. Zhao, Y. Wang, X. Kang, A. Wu, W. Yin, Y. Tang, J. Wang, M. Zhang, Y. Duan, Y. Huang, *Chem Sci.* **2018**, 9, 2674.

[7] K. Duval, H. Grover, L. Han, Y. Mou, A. Pegoraro, J. Fredberg, Z. Chen, *Physiology* **2017**, 32, 266.

[8] A. Riedl, M. Schlederer, K. Pudelko, M. Stadler, S. Walter, D. Unterleuthner, C. Unger, N. Kramer, M. Hengstschläger, L. Kenner, D. Pfeiffer, G. Krupitza, H. Dolznig, *J. Cell Sci.* **2017**, 130, 203.

[9] D. Priwitaningrum, J. Blondé, A. Sridhar, J. van Baarlen, W. Hennink, G. Storm, S. Le Gac, J. Prakash, *J. Control. Release* **2016**, 244, 257.

[10] J. Grolman, D. Zhang, A. Smith, J. Moore, K. Kilian, *Adv. Mater.* **2015**, 27, 5512.

[11] a) W. Jia, P. Gungor-Ozkerim, Y. Zhang, K. Yue, K. Zhu, W. Liu, Q. Pi, B. Byambaa, M. Dokmeci, S. Shin, A. Khademhosseini, *Biomaterials* **2016**, 106, 58; b) B. Byambaa, N. Annabi, K. Yue, G. Trujillo-de Santiago, M. Alvarez, W. Jia, M. Kazemzadeh-Narbat, S. Shin, A. Tamayol, A. Khademhosseini, *Adv. Healthc. Mater.* **2017**, 6, 16; c) J. Yang, Y.S. Zhang, Yue K, Khademhosseini A., *Acta Biomater.* **2017**, 57; d) H. Kang, S. Lee, I. Ko, C. Kengla, J. Yoo, A. Atala, *Nat. Biotechnol.* **2016**, 34, 312; e) K. Zhu, S. Shin, T. van Kempen, Y. Li, V. Ponraj, A. Nasajpour, S. Mandla, N. Hu, X. Liu, J. Leijten, Y. Lin, M. Hussain, Y. Zhang, A. Tamayol, A. Khademhosseini, *Adv. Funct. Mater.* **2017**, 27, 12.

[12] M. Noh, S. Oh, E. Ahn, Y. Kim, T. Jung, S. Jung, K. Kim, J. Lee, K. Lee, K. Moon, *BMC Cancer* **2017**, 17.

[13] W. Liu, Y.S. Zhang, M.A. Heinrich, F. De Ferrari, H. Jang, S. Bakht, M. Alvarez, J. Yang, Y. Li, G. Trujillo-de Santiago, A. Miri, K. Zhu, P. Khoshakhlagh, G. Prakash, H. Cheng, X. Guan, Z. Zhong, J. Ju, G. Zhu, X. Jin, S. Shin, M. Dokmeci, A. Khademhosseini, *Adv. Mater.* **2017**, 29, 3.

[14] W. Liu, M.A. Heinrich, Y. Zhou, A. Akpek, N. Hu, X. Liu, X. Guan, Z. Zhong, X. Jin, A. Khademhosseini, Y. Zhang, *Adv. Healthc. Mater.* **2017**, 6, 12.

[15] A. Poh, M. Ernst, *Front. Oncol.* **2018**, 8, 49.

[16] a) A. Chang, J. Miska, D. Wainwright, M. Dey, C. Rivetta, D. Yu, D. Kanojia, K. Pituch, J. Qiao, P. Pytel, Y. Han, M. Wu, L. Zhang, C. Horbinski, A. Ahmed, M. Lesniak, *Cancer Res.* **2016**, 76, 5671; b) B. Lu, Y. Zhou, Z. Su, A. Yan, P. Ding, *Mol. Med. Rep.* **2017**, 16, 3387.

[17] a) J. Drost, H. Clevers, *Nat. Rev. Cancer* **2018**, 18, 407; b) J. Hoarau-Véchot, A. Rafii, C. Touboul, J. Pasquier, *Int. J. Mol. Sci.* **2018**, 19, 1.

[18] P. Scodeller, L. Simón-Gracia, S. Kopanchuk, A. Tobi, K. Kilk, P. Säälik, K. Kurm, M. Squadrito, V. Kotamraju, A. Rinken, M. De Palma, E. Ruoslahti, T. Teesalu, *Sci. Rep.* **2017**, 7, 14655.

[19] H. Ge, L. Mu, L. Jin, C. Yang, Y. Chang, Y. Long, G. DeLeon, L. Deleyrolle, D. Mitchell, P. Kubilis, D. Lu, J. Qi, Y. Gu, Z. Lin, J. Huang, *Int. J. Cancer* **2017**, 141, 1434.

[20] B. Brücher, I. Jamall, *Cell Physiol. Biochem.* **2014**, 34, 213.

[21] K. Webb, V. Hlady, P. Tresco, *J. Biomed. Mater. Res.* **2000**, 49, 98.

[22] Y. Iwadate, *Oncol. Lett.* **2016**, 11, 1615.

[23] X. Guan, M. Hasan, S. Maniar, W. Jia, D. Sun, *Mol. Neurobiol.* **2018**, 55, 8.

[24] L. LexiDrugs, Lexi-Drugs, https://www.drugs.com/international/lexi.html, Accessed: 25 December 2018.

[25] K. Binnemars-Postma, R. Bansal, G. Storm, J. Prakash, *FASEB J.* **2018**, 32, 969.

[26] a) J. Conway, H. Pink, M. Bergquist, B. Han, S. Depee, S. Tadepalli, P. Lin, R. Crumrine, J. Binz, R. Clark, J. Selph, S. Stimpson, J. Hutchins, S. Chamberlain, B. TA., *J. Pharmacol. Exp. Ther.* **2008**, 326, 41; b) M. El-Gamal, S. Al-Ameen, D. Al-Koumi, M. Hamad, N. Jalal, C. Oh, *J. Med. Chem.* **2018**, 61, 5450.

Supporting Information

3D-Bioprinted Mini-Brain: A Glioblastoma Model to Study cellular interactions and therapeutics

Marcel Alexander Heinrich, Ruchi Bansal, Twan Lammers, Yu Shrike Zhang, Raymond Schiffelers, Jai Prakash**

METHODS

Chemicals & Materials

Gelatin from porcine skin (~300 g bloom, type A), methacrylic anhydride, 2-hydroxy-4′-(2-hydroxyethoxy)-2-methylpropiophenone (photoinitiator, PI), phalloidin-tetramethylrhodamine B isothiocyanate (phalloidin-TRITC) antibody, propidium iodide solution and Fluoroshield™ with DAPI were purchased from Sigma-Aldrich (St. Louis, MO, USA). Gelatin methacryloyl (GelMA) was synthesized according to previously published protocols at a high degree of methacryloyl substitution (~75%).[1] In brief, 10% w/v gelatin was dissolved in phosphate buffered saline (PBS, self-made) at 50 °C until a homogenous solution was obtained. Then 8% v/v of methacrylic anhydride were added to the solution drop-wisely. The solution was allowed to react for 2h under constant stirring before the reaction was stopped by adding MiliQ water. Then the GelMA solution was dialyzed against MiliQ water for a total duration of 4 days under constant stirring before being lyophilized and stored at -20°C until being used in the experiments. The degree of functionalization was determined by ^{1}H Nuclear Magnetic Resonance (NMR) (Varian Inova NMR Spectrometer, Palo Alto, CA, USA) (**Supplementary Figure S10**). Cell analysis reagents calcein AM, CellTracker Green CMFDA, CellTracker Orange CMRA, Alexa Fluor 488 antibody, Alexa Fluor 594 antibody and NucBlue Fixed Cell

Stain for 4',6-diamino-2-phenylindole (DAPI) were obtain from Thermofisher Scientific (Waltham, MA, USA). Gfap antibody was purchased from Santa Cruz Biotechnology (Dallas, TX, USA), Cd206 antibody was purchased from Abcam (Cambridge, MA, USA). All secondary antibodies were purchased from Dako Denmark A/S (Glostrup, Denmark).

Bioprinter Modification & Programming

The 3D bioprinter was customized from an existing 3D printer (UltiMaker 2 Go, UltiMaker, Geldermalsen, Netherlands). The original extrusion head was removed and replaced by a custom 3D-printed syringe holder that could hold two different syringes. Bioprinting was based on pressure-driven extrusion on supplied nitrogen gas. We used a custom-built valve-system to switch between the different syringes, allowing for rapid changing of the bioink and cells (all valves, tubes and connectors obtained from Landefeld Druckluft und Hydraulik GmbH, Kassel, Germany). The bioprinted structure was based on a model created in Blender (Blender Foundation, Amsterdam, Netherlands) and translated into a G-code using Cura (UltiMaker).

Bioink Optimization

Experiments to find the optimal concentration and ratio of GelMA and gelatin within the gel were based on the optimal GelMA stability and crosslinking time, and the gelatin concentration for optimal support after printing and gelation of the bioink. The optimum GelMA concentration was determined by preparing several different bioinks consisting of a GelMA concentration ranging from 1-4% w/v, 4% w/v gelatin, 10 % v/v fetal bovine serum (FBS, Lonza, Basel, Switzerland), 1 % v/v Penicillin/Streptomycin (Pen/Strep, Lonza) and 0.2 % w/v PI. Constructs were bioprinted using the modified bioprinter and crosslinked with UV light (λ 365nm, NailStar NS-01, NailStar Professional, London, UK) at 12 mW/cm^{-2} and 5 cm distance for either 0.5, 1, 2 or 3 min. The stability of the bioink was determined by

visual observation immediately after bioprinting as control, after 1.5 h incubation in PBS at 37 °C indicating non-successful crosslinking, and after 10 days incubation in PBS at 37 °C after bioprinting representing the setting during later experiments (**Supplementary Figure S1A & S1B**). Eventually the bioink displaying properties with the lowest GelMA concentration and lowest crosslinking time was chosen displaying point (iv) characteristics.

The optimum gelatin concentration was determined based on the gelation time, which was set to ≤ 20 min to avoid potential influence on cell viability and printability of the bioink. Several different bioinks were prepared consisting of 3% w/v GelMA, gelatin ranging from 2-6% w/v, 10% v/v FBS, 1 % v/v Pen/Strep and 0.2 % w/v PI. The bioinks were warmed up to 37°C for 15 min, transferred into transparent glass vials and placed on a roller at constant speed. Gelation time was determined by visual observation for a total duration of 20 min (**Supplementary Figure S1C**). Secondly, the gelation state was confirmed by transferring the bioink into glass vials, allowing gelation for 15 min and then turning the vials upside down to display the flow of the different bioinks (**Supplementary Figure S1D**). To investigate to printability, the bioinks were warmed up to 37°C for 15 min, transferred to a syringe (Terumo, Tokyo, Japan) equipped with a 30G blunt needle (Cellink, Gothenburg, Sweden) and allowed to gel for 15 min. Then the bioink was extruded following a straight line (**Supplementary Figure S1E & S1F**). The printability was determined by visual observation of the bioprinted line depending on the resolution and thickness.

Bioink Preparation for Experiments

The bioink for all experiments was prepared a maximum of 24h before use. First, 6.6 % w/v GelMA and 8.8 % w/v gelatin were dissolved in sterile Dulbecco's phosphate buffered saline (DPBS, Lonza) and warmed up to 37°C for 15 min before mixing (ratio of 1:1). Next, 10 % v/v FBS and 1 % v/v Pen/Strep were added to the bioink, resulting in a total concentration of

3 % w/v GelMA and 4 % w/v gelatin. Then 0.2 % w/v of PI were added to the bioink to enable later crosslinking of the construct. The bioink was stored at 4°C under dark conditions until experiments.

Bioink Characterization

Rheological characterization was performed with an Anton Paar rheometer (Physica MCR301, Anton Paar, Graz, Austria) equipped with a parallel disk (PP25, Ø 25mm, Anton Paar). Prior to all measurements the bioink was warmed up to 37°C. Spacing between the parallel disk and bottom plate was set constant to 1 mm for all measurements. For measurements depending on time (10 min, fixed measurement points at every 10 s) the strain was set constant to 5% and the angular frequency to 10 s^{-1}. For experiments at 37°C the measurement was started immediately after applying the bioink. For measurements at 20°C, the bioink was allowed for gelation for 15 min before starting the measurement. For rheological characterization depending on the angular frequency the strain was set to constant to 5% and the angular frequency ranged from 0.1 to 100 s^{-1} with various measurement points in logarithmic scale (initial 10 s, final 10 s, 10 points/ decade) for a total duration of 310 s.

For scanning electron microscopy (SEM), cubic structures (4mm x 4mm x 1.5 mm, W x L x H) were bioprinted without cells. The bioprinted constructs were incubated at 37°C in DPBS for 24 h allowing the gelatin to leak out of the constructs before frozen in liquid nitrogen and lyophilized for 2 days. Afterwards, the freeze-dried samples were broken in liquid nitrogen to receive a cross-section of the bioprinted constructs, gold-sputtered (Sputter Coater 108 Auto, Cressington Scientific Instruments, Watford, UK) and imaged with a scanning electron microscope (JSM-IT100, JEOL, Tokyo, Japan).

Cell Culture

GL261 glioblastoma cells (Leibniz-Institute DSMZ, Deutsche Sammlung von Mikroorganismen und Zellkulturen GmbH, Braunschweig, Germany) and RAW264.7 macrophages (American Type Culture Collection, ATCC, Manassas, VA, USA) were cultured according standard procedures. In brief, GL261 glioblastoma cells were cultured in Dulbecco's Modified Eagle Medium (DMEM, High Glucose, HyClone, Thermofisher Scientific) containing 10 % v/v FBS and 1 % v/v Pen/Strep. RAW 264.7 macrophages were cultured in Roswell Park Memorial Institute (RPMI) medium (Lonza) containing 200mM L-Glutamine (Lonza), 10 % v/v FBS and 1 % v/v Pen/Strep. Both cell types were cultured in a humidified atmosphere of 5% CO_2 at 37°C and split at 80% confluence.

Cell Bioprinting

For all cell bioprinting experiments the prepared bioink was warmed up to 37°C and mixed with cells to achieve a homogenous solution. For all experiments a cell density of $2x10^6$ GL261 glioblastoma cells/ mL and $3x10^6$ RAW264.7 macrophages/ mL was used. Afterwards the cell-laden bioink was transferred into a sterile syringe (Terumo) equipped with a 30G blunt needle (Cellink) and allowed to gel for 15 min at RT. Cell laden mini-brains were bioprinted onto a sterile microscope slide via pressure-based extrusion and immediately crosslinked by exposure to UV light (λ 365nm, 12 mW/cm -2) for 2 min. The bioprinted mini-brains were washed three times in DPBS before placed in the cell specific culture medium and transferred to the incubator. For experiments including mini-brains containing both cell types were mixed in a cell culture medium containing DMEM and RPMI culture media at a ratio of 1:1 in all 2D, 3D and 3D co-cultures. Approximately 1h and 24h after bioprinting the culture medium was refreshed. Further refreshments took place every alternate day.

Cell Viability

To determine the viability of cells after bioprinting a Calcein AM(LIVE)/ Propidium Iodide (DEAD) staining on bioprinted mini-brains was performed. In brief, mini-brains containing GL261 glioblastoma cells and RAW264.7 macrophages were bioprinted and cultured as previously mentioned. Immediately, 4 and 10 days after bioprinting the cells were washed twice with DBPS before incubated with 2 µM Calcein-AM to stain alive cells and 25 µg/mL propidium iodide to stain dead cells for 20 min at RT and immediately imaged with fluorescence microscopy (EVOS Cell Imaging System, Thermofisher Scientific). Quantification was performed by counting alive and dead cells using ImageJ (Wayne Rasband, NIH, MD).

Cell Metabolic Activity

The metabolic activity of cells was measured 1, 4, 7 and 10 days after bioprinting. To monitor the activity, 30 µL of Alamar Blue dye (Invitrogen, Carlsbad, USA) in 300 µL of culture medium was added per well. After 24h, the fluorescent signal was measured using a VIKTOR™ plate reader (Perkin Elmer, Waltham, Massachusetts).

Gene Expression in Bioprinted Mini-Brains

To evaluate the gene expression, mini-brains containing either GL261 glioblastoma cells or RAW264.7 macrophages were bioprinted as previously mentioned and cultured for 4 days. The time point for 4 days was chosen to prevent cross-contamination between the cells as macrophages displayed rapid growth and evasion out of the gel at 5 days and higher. Additionally, GL261 glioblastoma cells and RAW264.7 macrophages were seeded in a 12 well plate at a cell density of $1x10^5$ cells/ well and $1x10^6$ cells/ well, respectively, and cultured for 3 days serving as control. Cells in 3D-bioprinted mini-brains were cultured one day longer to allow cells to recover from bioprinting and the results of gelatin leakage from the construct. Before RNA isolation 3D-bioprinted mini-brains were incubated in culture

medium containing 200 µg/mL collagenase (from Clostridium Histolyticum, activity ≥ 800 units/mg, Sigma-Aldrich) for 45 min at 37°C to degrade the bioink matrix enabling simple RNA isolation. The RNA from cells obtained from the 2D monolayer and from the 3D-bioprinted mini-brains was isolated using the GenElute™ Mammalian Total RNA Miniprep Kit (Sigma Aldrich) and the RNA amount was measured by Nanodrop® ND-1000 spectrophotometer (ThermoScientific). Subsequently, cDNA was synthesized with iScript™ cDNA synthesis Kit (BioRad, Venendaal, Netherlands). 10 ng cDNA were used for each PCR reaction. The real-time PCR primers (**Supplementary Tables S2 & S3**) were purchased from Sigma Aldrich. Quantitative real time PCR was performed using 2x SensiMix SYBR and Fluorescein Kit (Bioline GmbH, Luckenwalde, Germany) using a BioRad CFX384 Real-Time PCR detection system (BioRad). Gene levels were normalized to the expression of the house-keeping gene Gapdh.

Gene Expression in Co-Culture of separately Bioprinted Mini-Brains

To investigate the paracrine signaling between GL261 glioblastoma cells and RAW264.7 macrophages, mini-brains containing either GL261 glioblastoma cells or RAW264.7 macrophages were bioprinted as described previously. After bioprinting, these mini-brains were cultured in the same well separated by a custom-made divider. Similarly, mini-brains from each cell type were cultured alone serving as single cell control. Additionally, GL261 glioblastoma cells and RAW264.7 macrophages were seeded in a 2D monolayer as previously described and cultured for 3 days. After 4 days of culturing the co-cultured mini-brains were separated and prepared for RNA isolation similar to previous experiments. 2D and 3D controls were also prepared for RNA isolation and analysis. RNA isolation, cDNA synthesis and real-time PCR were performed as previously described. Gene levels were normalized to the expression of the house-keeping gene Gapdh.

Immunofluorescent Staining in Co-Culture of separately Bioprinted Mini-Brains

GL261 glioblastoma and RAW264.7 containing mini-brains were 3D co-cultured, 3D single cultured and 2D cultured as previously described. After 4 days of culture the separated co-cultured and single-cultured mini-brains were fixed in 4% formaldehyde for 30 min, incubated in 1% poly vinyl alcohol (PVA, Sigma-Aldrich) for 3h at RT and snap frozen in cryomatrix (Shandon™ Cryomatrix™ embedding resin, Thermofisher Scientific) using 4-methylbutane (Acros Organics, Geel, Belgium) before sectioned into 20 µm thick slices for analysis. Immunofluorescent staining of sectioned mini-brains was performed using standard protocols. In brief, sections were permeabilized with ice-cold methanol for 10 min at -20°C and washed three times with PBS before incubation with primary antibody overnight at 4°C. On the next day, the cells were washed and incubated with secondary antibody in PBS containing 5 % v/v normal mouse serum (Sigma-Aldrich) for 3h. After washing, the cells were incubated with tertiary antibody conjugated to fluorescent Alexa Fluor 488 or 564 in PBS containing 5 % v/v normal mouse serum for 3h. Finally, the sections were mounted with Fluoroshield™ with DAPI and imaged with fluorescent microscopy. As control, 2D monolayers were also analyzed with immunofluorescent staining using standard staining protocols for 2D cultures. In brief, cells were fixed with 4% formaldehyde for 10 min, washed three times with PBS and incubated with primary antibody for 1h. Afterwards the cells were washed and incubated with secondary antibody followed by fluorescent tertiary antibody in PBS containing 5 % v/v normal mouse serum for 1h before stained with NucBlue fixed cell stain for DAPI for 10 min and imaged with fluorescent microscopy. All incubations, if not mentioned otherwise, were performed at RT.

Phalloidin/DAPI Staining for Cell Attachment

For 2D monolayers GL261 glioblastoma cells and RAW264.7 macrophages were seeded into a tissue-culture treated 48 well plate (Cellstar, Greiner Bio One, Kremsmünster, Austria) at a seeding density of $25x10^3$ cells/ well and $100x10^3$ cells/ well, respectively. For investigating the attachment of cells onto bioprinted constructs, bioink without cells was extruded directly into a 48 well plate and crosslinked for 2 min under UV light. After crosslinking GL261 glioblastoma cells and RAW264.7 macrophages were seeded on top of the gels with the same density as used in 2D culture. After culturing for 3 days, the cells were washed twice with DPBS and fixed with 4% formaldehyde (Sigma-Aldrich) for 10 min before stained with phalloidin-TRITC/DAPI using standard protocols. In brief, the cells in monolayer and on top of the bioprinted construct were washed before incubated in 0.1% Triton-X100 in PBS for 15 min to permeabilize the cell membrane. After washing three times with PBS non-active sites were blocked using 1 % w/v bovine serum albumin (BSA, VWR International, Radnor, PA, USA) in PBS for 1h. Finally, the cells were incubated with phalloidin-TRITC antibody in 0.1 % w/v BSA solution for 1h followed by washing once with PBS and incubating with NucBlue Fixed Cell Stain for DAPI for 10 min before storing in PBS. Afterwards the cells were imaged by fluorescent microscopy. All incubations were performed at RT.

Scanning Electron Microscopy for Cell Attachment

GL261 glioblastoma cells and RAW264.7 macrophages were seeded on top of extruded constructs in a 48 well plate as previously described. After culturing for 3 days, the cells on top of the gel were fixed with 2.5% glutaraldehyde (Electron Microscopy Sciences, Hatfield, PA, USA) for 1h at RT and additional 24h at 4°C. Afterwards, the constructs with cells were frozen in liquid nitrogen and lyophilized for 2 days. The dried constructs were then gold-sputtered and prepared for SEM imaging as previously described.

Cell Migration/ Recruitment

To investigate the specific migration of GL261/RAW264.7 towards the opposite cell types we performed a custom-designed migration assay. Mini-brains containing either GL261 glioblastoma cells or RAW264.7 macrophages were bioprinted and cultured as previously mentioned. Migration was investigated after culturing the mini-brains for 4 days in case of RAW264.7 macrophages or 10 days in case of GL261 glioblastoma cells allowing the cells to proliferate until they display free migration out of the gel. For investigating the migration, the mini-brains were placed into a 48 well plate without cells, with a monolayer of the similar cell type and with a monolayer of the opposite cell type. For this assay the cells in monolayer were seeded 1 day prior to the experiment with a cell density of $50x10^3$ or $250x10^3$ cells/well for Gl261 glioblastoma cells or RAW264.7 macrophages, respectively. Before placing the mini-brains in top of the monolayer, the cells in the mini-brains were incubated with CellTracker Green CMFDA and the cells in monolayer were incubated with CellTracker Orange CMRA for 1h at 37°C. After 24h of direct cell-to-cell contact between the mini-brains and the monolayer, the mini-brains were removed, the monolayer washed and incubated with NucBlue fixed cell stain for 10 min before directly imaged using fluorescence microscopy. The degree of migration was based on the quantity of green-labelled cells on top of the orange-labelled monolayer, analyzed using ImageJ.

Gene Expression in Co-culture of Bioprinted Mini-Brains containing GL261 and RAW264.7 in a Single Construct

To investigate the effects of direct cell-to-cell contact on the gene expression, mini-brains consisting of RAW264.7 macrophages including a cavity containing GL261 glioblastoma cells (**Figure 1**) were bioprinted. Similarly, 3D mini-brains containing only RAW264.7 macrophages or a cavity of GL261 glioblastoma cells were bioprinted and 2D monolayers of cells were seeded as described earlier. After 4 days of culture the area containing tumor cells was resected to separate the two cells types before matrix degradation in medium containing

collagenase and RNA isolation. RNA isolation, cDNA synthesis and real-time PCR for 3D co-cultured, single cultured and 2D cultured cells was performed according to previously mentioned protocols. Gene levels were normalized to the expression of the house-keeping gene Gapdh. Additionally, gene levels were normalized to the content of the GL261 glioblastoma cells in constructs used for RAW264.7 macrophage gene expression based on the expression of Gfap, eventually to be considered negligible (**Supplementary Figure S7**). The content of RAW264.7 macrophages in constructs used for GL261 glioblastoma cell gene expression is normalized to the expression of F4/80. Furthermore, one sample of the opposite cell type was analyzed for each primer to determine the expression in the specific cell type and to normalize accordingly. In more detail, we corrected the F4/80 value in the 3D co-culture with the value in the 3D single culture, where no macrophages were involved, to obtain the factor for standardization (F macrophage (F_M)). In cultures where we detected higher expression of the target gene in macrophage single cultures we considered the measured expression to be mainly influenced by macrophages and used formula (1):

$$CE_G = {ME_G}/{F_M} \quad (1)$$

Where CE_G is the corrected expression in glioblastoma cells, ME_G is the measured expression in glioblastoma cells and F_M is the standardization factor for the macrophage content to obtain the corrected expression for glioblastoma cells only. In cultures where we observed a higher expression of the specific target in glioblastoma cell single cultures, we considered the ME_G to be decreased due to the lack of expression in macrophages and we used formula (2) to correct for the expression in glioblastoma cells.

$$CE_G = {ME_G}/{F_M{}^{-1}} \quad (2)$$

In cultures where we did not detect any difference in the expression levels for both cell types, we did not correct the measured expression as both cell types are considered to have equal influence on the expression.

Transcriptome expression analysis in the human cohort from the public database

We selected and downloaded human gliomas gene expression datasets from the Expression Omnibus database (GEO). GSE16011 dataset comprises 8 control samples and gliomas from 159 GBM Grade IV patients.[2] We used GEO2R to assess the expression of different mRNA expression in gliomas versus control samples and plotted the normalized gene expression levels.

Survival analysis in the human cohort from the public database

For the patient survival analysis we selected a dataset from The Cancer Genome Atlas (TCGA)[3] including 577 GBM patients that have been followed for a duration of 6 years in the online tool PROGgeneV2 from Goswami and Nakshatri[4] to determine the gene-dependent survival of all patients in the cohort study. Hereby, we compared the low versus high expression of specific genes found upregulated in GBM patients independent from age or gender. The classification between low and high expression was done by the software based on the median gene expression of the specific marker.[5]

BNCU treatment in 3D bioprinted monocultured GL261 and RAW264.7 mini-brains

Bioprinted mini-brains were treated with BCNU ranging from 0 – 1000 µM after 4 days of culturing to mimic the experimental conditions as used in later experiments. In addition, GL261 and RAW264.7 were seeded conventionally in a 2D monolayer and treated one day after seeding and treated with concentrations of BCNU ranging from 0 – 400 µM to serve as 2D control. The IC_{50} for all experiments was determined by Alamar Blue assay measured 48h

after treatment with BCNU and normalized to the metabolic activity on the day of treatment. The final IC_{50} was determined by creating a trend line of the measurement points and mathematically determine the IC_{50}.

BCNU treatment in bioprinted co-cultured RAW264.7/GL261 mini-brains

Bioprinted mini-brains containing RAW264.7/GL261 in a single construct as described previously were cultured for a duration of 4 days before the different cell types were separated for further culture. Immediately after separation the metabolic activity of the individual parts was determined by Alamar Blue assay as previously described, before treated with either vehicle or 550 µM BCNU. After 48h the metabolic activity of the individual parts were measured again and normalized to the day of treatment to determine the effect of vehicle- and BCNU treatment

AS1517499 and BLZ945 treatment in bioprinted co-cultured RAW264.7/GL261 mini-brains

Bioprinted mini-brains containing RAW264.7/GL261 in a single construct as described previously were cultured for a duration of 4 days and treated with either vehicle, 250 nM AS1517499 [6] (Axon Medchem, Groningen, Netherlands) or 1 µM BLZ945 [7] (Bio-Connect BV, Huissen, Netherlands) on day 1 and day 3 post-bioprinting before the different cell types were separated for further culture. Immediately after separation the metabolic activity of the individual parts was determined by Alamar Blue assay as previously described, before further culture of the individual parts. After 48h the metabolic activity of the individual parts were measured again and normalized to the day of treatment to determine the effect of AS1517499 or BLZ945 on the individual cells.

Gene expression analysis after AS1517499 and BLZ945 Treatment

Bioprinted mini-brains containing RAW264.7/GL261 in a single construct as described previously were cultured for a duration of 4 days and treated with either vehicle, 250 nM AS1517499 or 1 μM BLZ945 on day 1 and day 3 post-bioprinting before the different cell types were separated and analyzed for gene expression as previously described. Mini-brains containing only GL261 cells were also treated similarly to exclude possible effects on GL261 cells alone.

Graphs & Statistical Analysis

All graphs were made using GraphPad Prism Vol.5 (GraphPad Software Inc., San Diego, CA) based on calculations using Microsoft Excel (Microsoft, Redmond, WA, USA). All values are expressed as mean ± standard error of the mean (SEM). Statistical significance of the results was performed by either two-tailed unpaired student's t-test for comparison between two treatment groups or two-way ANOVA for to compare multiple treatment groups. Statistical significance between two patient groups in survival analysis was performed by Log-rank (Mantel-Cox) test. Significant difference was determined for a p-value of $*p < 0.05$, $**p < 0.01$ and $***p < 0.001$, respectively.

Supplementary References

[1] K. Yue, G. Trujillo-de Santiago, M. Alvarez, A. Tamayol, N. Annabi, A. Khademhosseini, *Biomaterials* **2015**, 73, 254.

[2] L. Gravendeel, M. Kouwenhoven, O. Gevaert, J. de Rooi, A. Stubbs, J. Duijm, A. Daemen, F. Bleeker, L. Bralten, N. Kloosterhof, B. De Moor, P. Eilers, P. van der Spek, J. Kros, P. Sillevis Smitt, M. van den Bent, P. French, *Cancer Res.* **2009**, 69, 9065.

[3] T. C. G. Atlas, cancergenome.nih.gov, Accessed: 25 December 2018.

[4] C. G. a. H. Nakshatri, *BMC Cancer* **2014**, 14.

[5] C. G. a. H. Nakshatri, J. *Clin. Bioinforma.* **2013**, 3.

[6] K. Binnemars-Postma, R. Bansal, G. Storm, J. Prakash, *FASEB J.* **2018**, 32, 969.

[7] S. Rebelo, C. Pinto, T. Martins, N. Harrer, M. Estrada, P. Loza-Alvarez, J. Cabeçadas, P. Alves, E. Gualda, W. Sommergruber, C. Brito, *Biomaterials* **2018**, 163, 185.

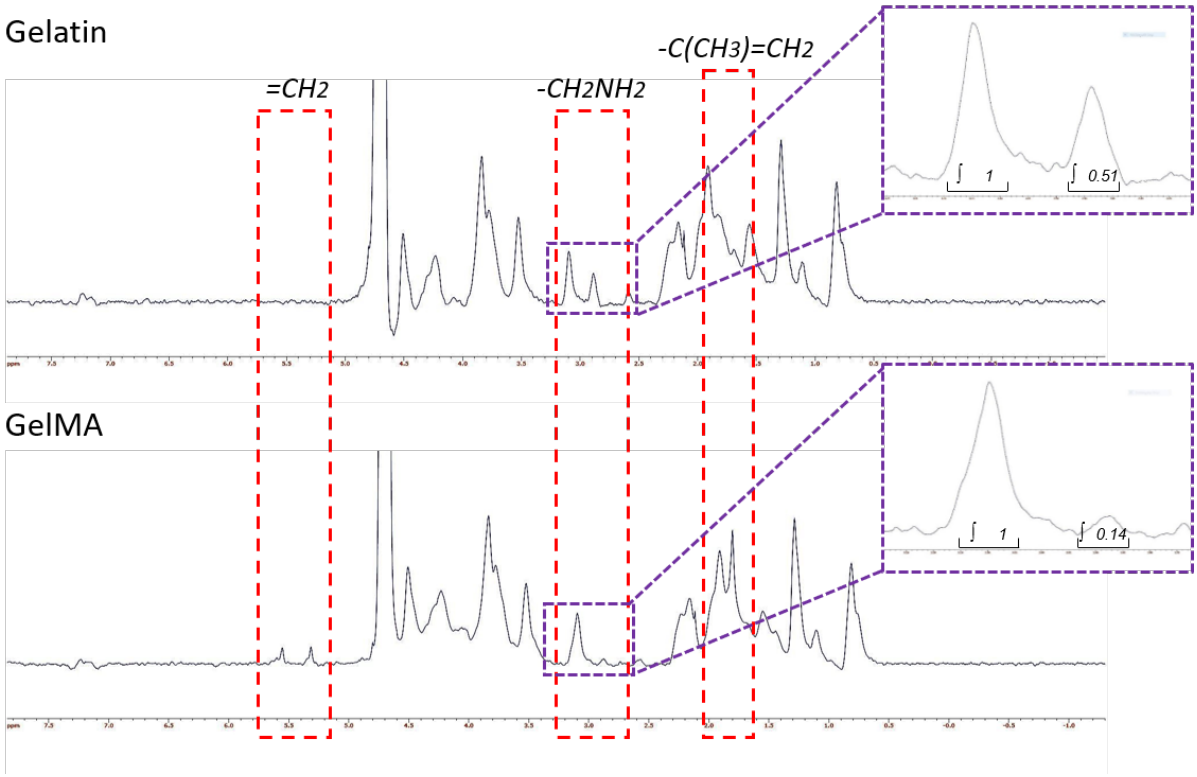

Supplementary Figure S1 NMR spectra of gelatin and gelatin-methacryloyl. (Top) NMR spectrum of gelatin with focus on unreacted lysine group. (Bottom) NMR spectrum of GelMA with focus on reacted lysine group indicating the degree of functionalization (Df).

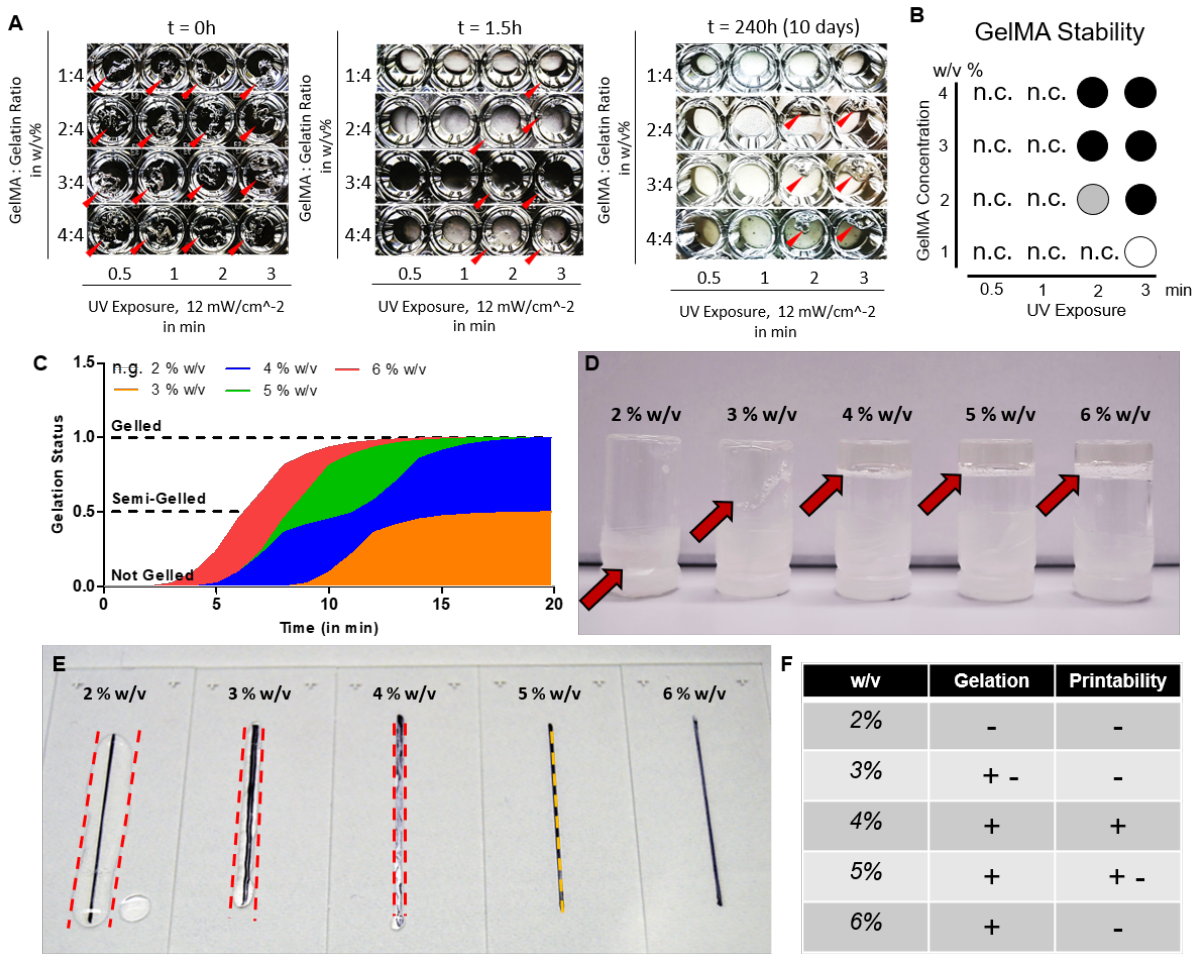

Supplementary Figure S2 Stability and gelation of bioink. A, B) Bioink containing 1-4 w/v% GelMA, 4 w/v% gelatin and 0.2 w/v% PI at different exposure times to UV light. A) Visual stability of the bioink at point of crosslinking (t=0h), after 1.5h incubation in PBS at 37°C , and after 250h (10 days) of incubation in PBS at 37°C. Red arrows display location and presence of crosslinked construct. B) Summarized results for the GelMA stability optimization displaying the stability of GelMA after 10 days of incubation in PBS at 37°C (n.c. = non-crosslinked, white circle = crosslinked but not stable for 10 days, grey circle = stable for 10 days but lost rigidity, black circle = fully stable after 10 days without losing rigidity. C – F) bioinks consisting of 3 %w/v GelMA, 2-6 %w/v gelatin and 0.2 %w/v PI. C) Gelation time for different bioinks. Status "semi-gelled" indicates the begin of gelation where the viscosity of the bioink increases, status "gelled" indicates a fully gelled/ solidified bioink (n.g. = no gelation).

D) Bioinks after 15 min of gelation at room temperature. Arrows indicate location of the bioink in glass vials. E) Extruded lines of different bioinks at constant speed and constant pressure after 15 min of gelation. Red lines indicate thickness of the extruded lines. Orange line indicates hardly present extruded line. F) Summarized results for gelatin support optimization displaying the bioinks able to gel in 15 min at RT while still being printable ("-" not suitable, "+-" limited, "+" optimal).

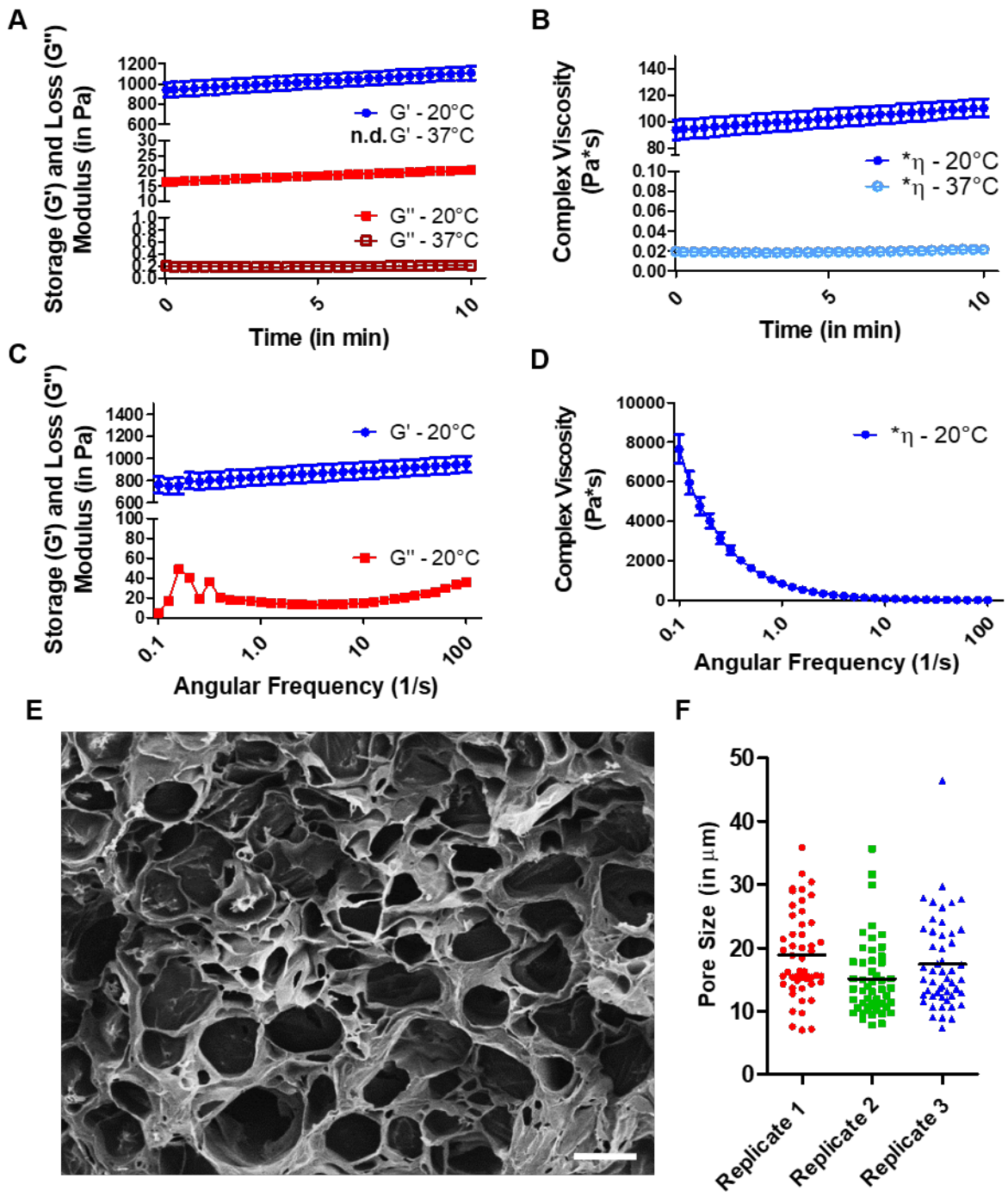

Supplementary Figure S3 Characterization of the optimized 3 w/v% GelMA- 4 w/v% gelatin bioink. A, B) Rheology measurement of GelMA (3 w/v.%)-gelatin (4 w/v.%) bioink for the storage (G') and loss (G'') moduli in relation to (A) time and (B) angular frequency (n.d. = not detected). C, D) Rheology measurement for the viscosity in relation to (C) time and (D) angular frequency. E) SEM images of the bioprinted crosslinked construct after incubation for

24 h at 37 °C, scale bar = 20 μm. F) Measured pore size for 3 independent samples (50 pores/ sample, longest distance).

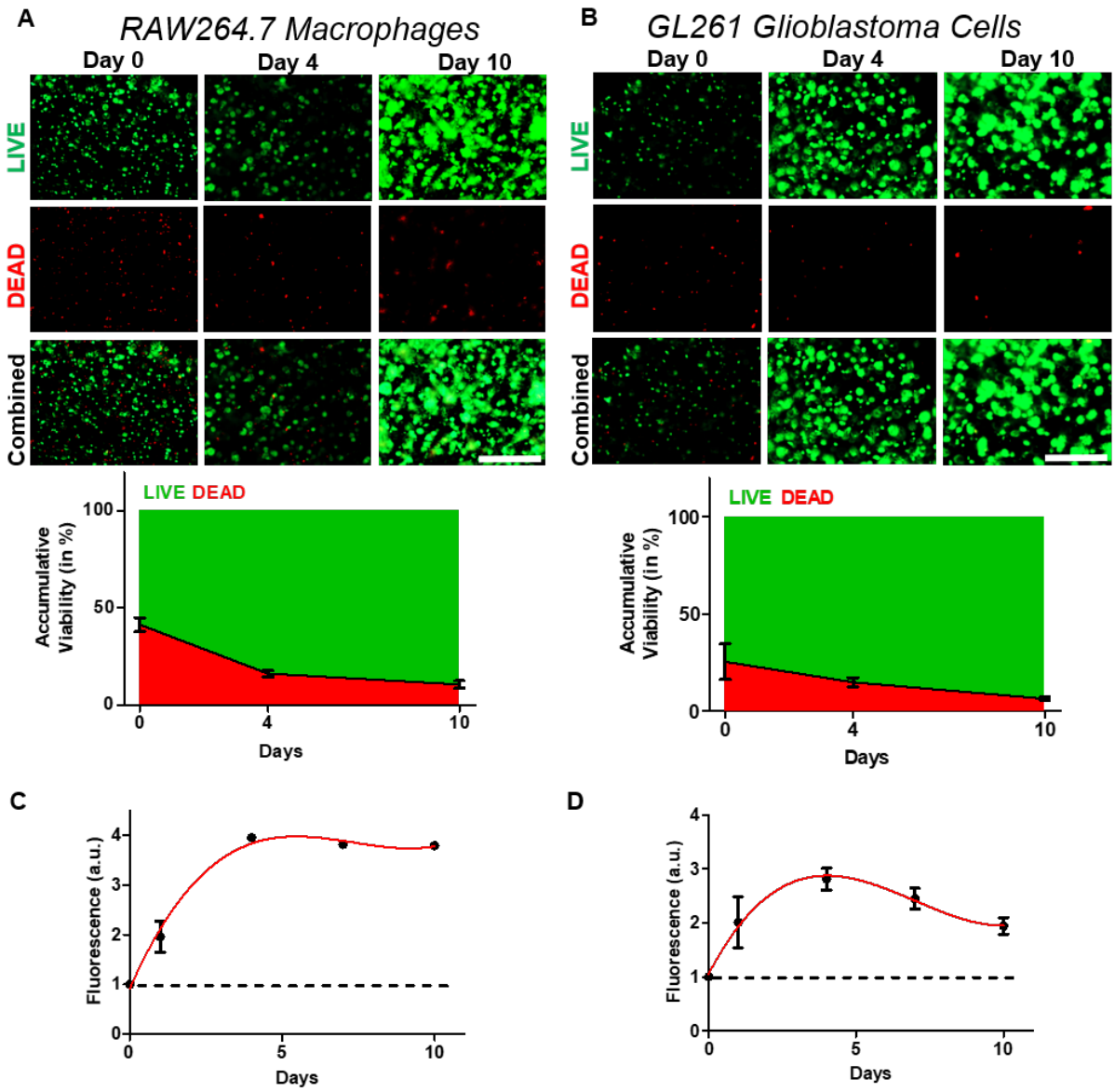

Supplementary Figure S4 Viability and metabolic activity of bioprinted RAW264.7 macrophages and GL261 glioblastoma cells. A, B) LIVE/DEAD staining and quantitative analysis of bioprinted (A) RAW264.7 macrophages and (B) GL261 glioblastoma cells based, scale bar = 1000 µm. C, D) Metabolic activity of bioprinted (C) RAW264.7 macrophages and (D) GL261 glioblastoma cells.

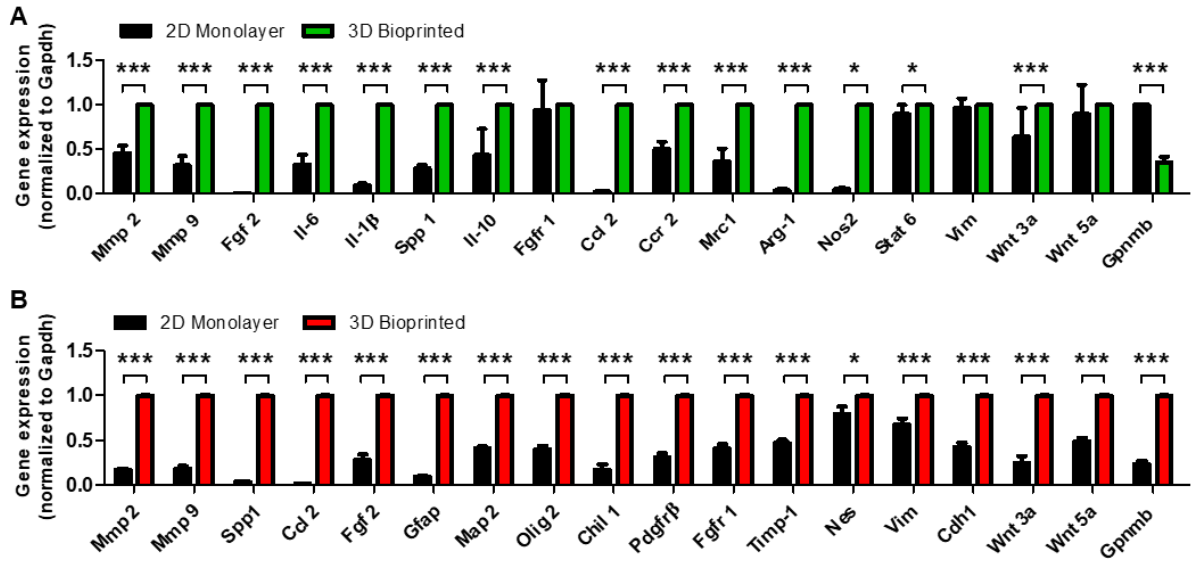

Supplementary Figure S5 Gene expression of bioprinted RAW264.7 macrophages and GL261 glioblastoma cells versus 2D monolayer control. A, B) Gene expression profiles of 2D monolayer cultures versus 3D-bioprinted mini-brains containing either (A) RAW264.7 macrophages or (B) GL261 glioblastoma cells (n = 6). Data represent mean ± SEM for at least 3 independent experiments, unless noted otherwise. Statistical analysis was performed by two-tailed unpaired student's t-test. *$p < 0.05$, ***$p < 0.001$. Data was used to serve as 2D and 3D control in Figure 2 and 3 of the main manuscript.

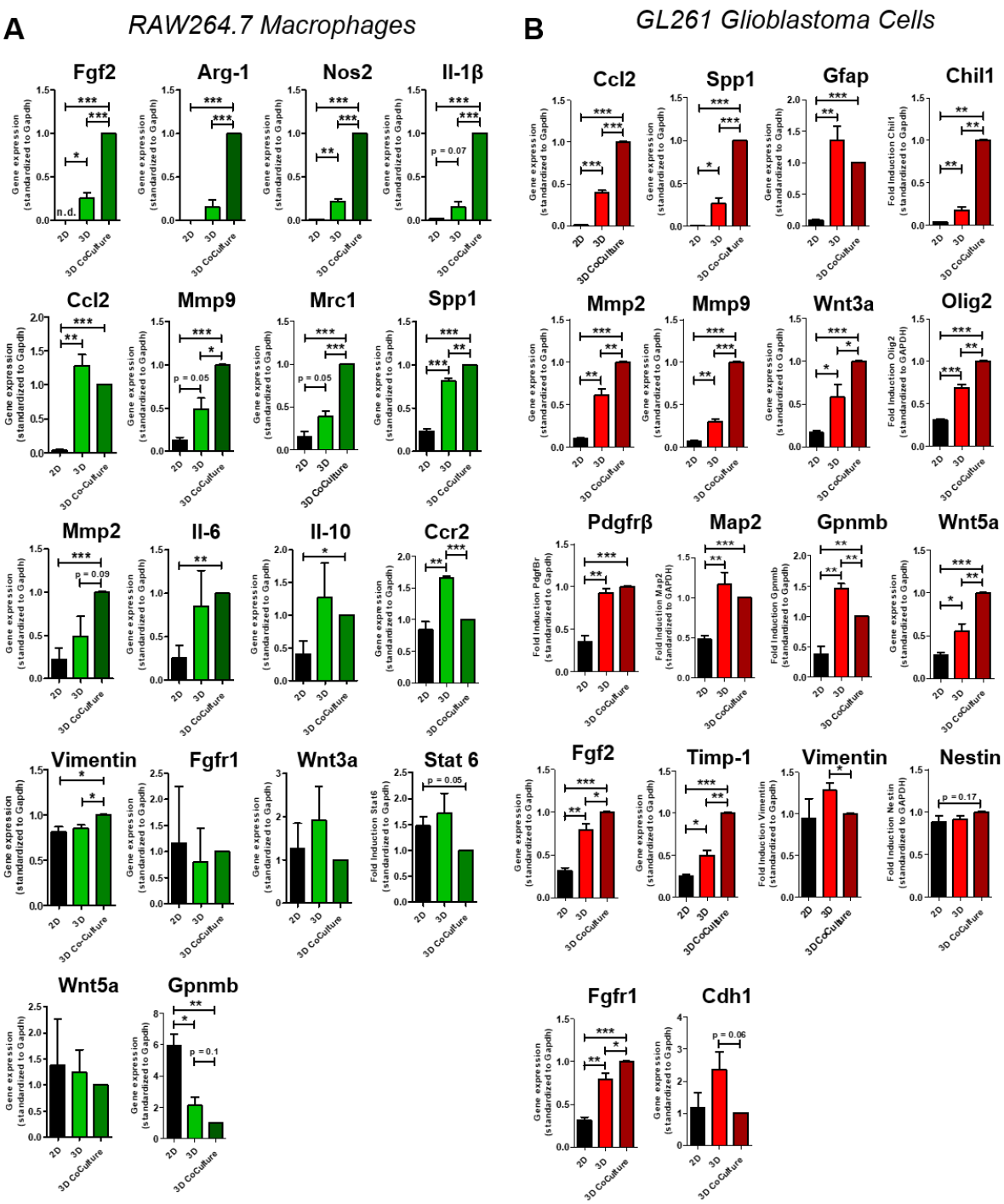

Supplementary Figure S6 Gene Expression in separately bioprinted RAW264.7 Macrophages in 2D, 3D single and 3D co-culture with GL261 cells. A) Heat map of expressed genes in RAW264.7 macrophages. B) Expression of different genes in RAW264.7 macrophages for 2D monolayer, 3D single bioprinted and 3D separately bioprinted co-culture with GL261. Data represent mean ± SEM for at least 3 independent experiments. Statistical

analysis was performed by two-tailed unpaired student's t-test. *$p < 0.05$, **$p < 0.01$, ***$p < 0.001$.

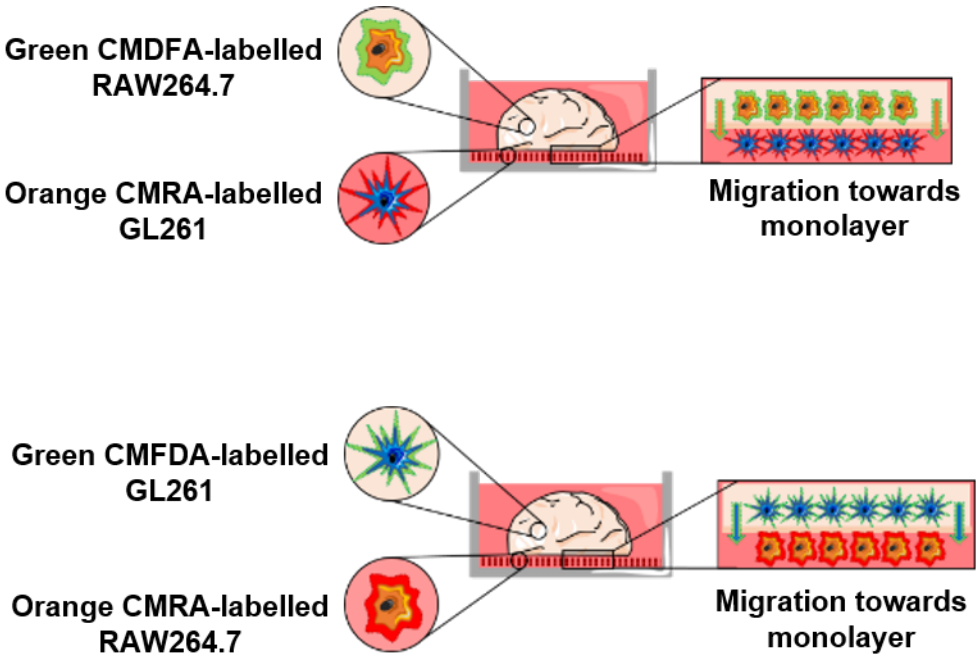

Supplementary Figure S7 Schematic representation of the custom designed migration assay (results shown in figure 3 of the main manuscript) for (top) RAW264.7 migration and (bottom) GL261.

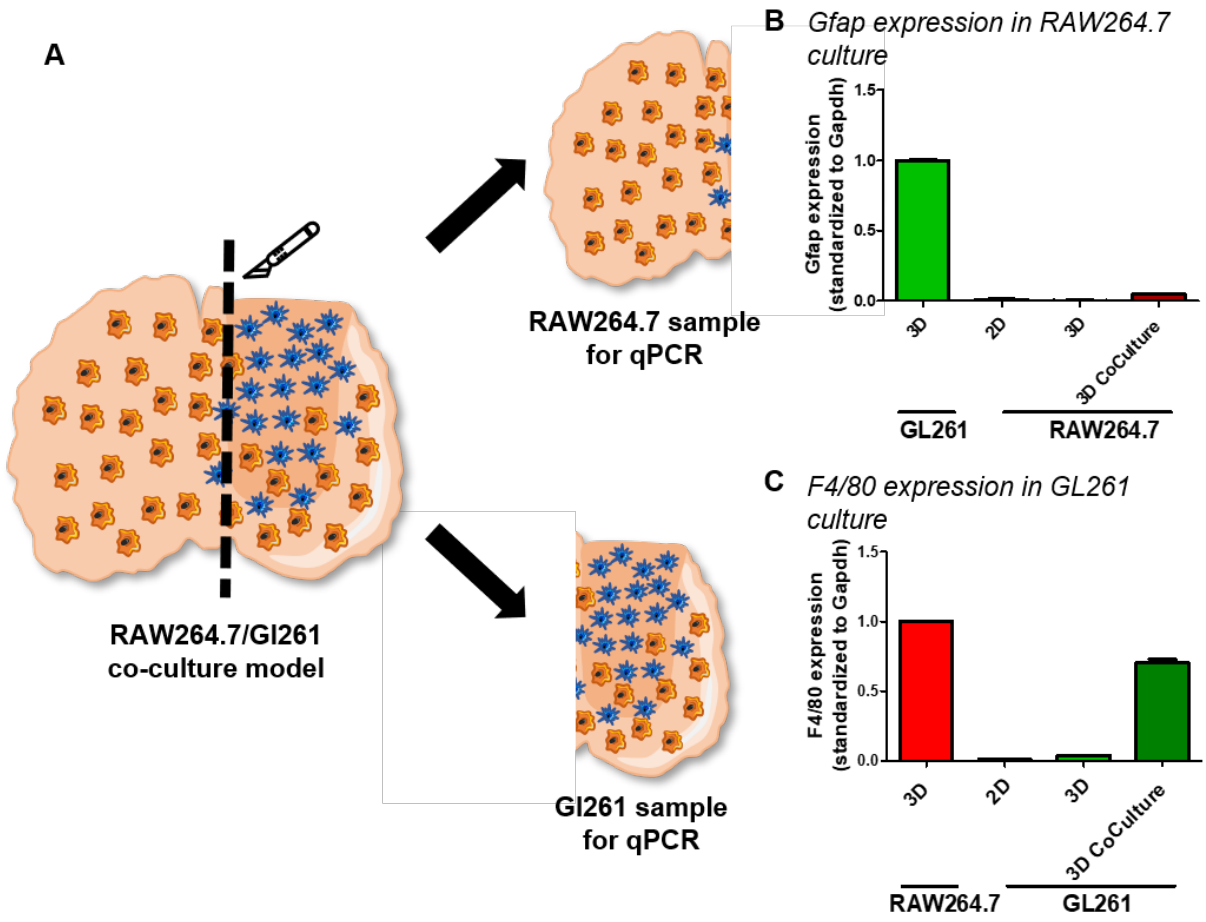

Supplementary Figure S8 Gene expression of F4/80 and Gfap in 3D RAW264.7/GL261 co-culture model. A) Schematic illustration of dividing the brain for further analysis for gene expression displaying the source of contamination from unwanted cells. B) Gfap expression in RAW264.7/GL261 co-culture model used for RAW264.7 analysis with respect to Gfap expression in single 3D GL261 culture. C) F4/80 expression in RAW264.7/GL261 co-culture model used for GL261 analysis with respect to F4/80 expression in single 3D RAW264.7 culture. Data represent mean ± SEM for at least 3 independent experiments.

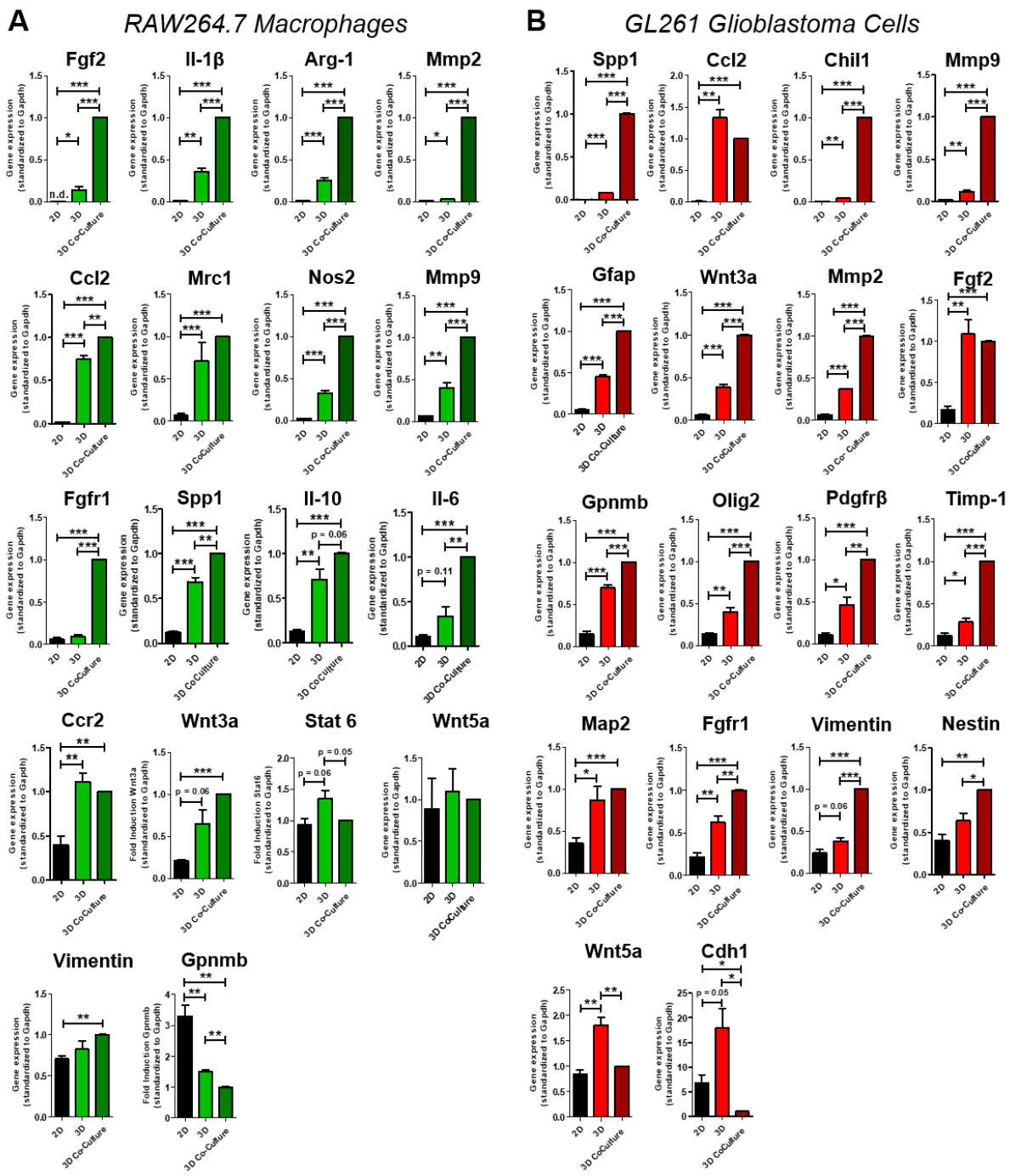

Supplementary Figure S9 Gene Expression of RAW264.7 Macrophages in 2D, 3D single and 3D RAW264.7/GL261 co-culture model. A) Heat map of expressed genes in RAW264.7 macrophages. B) Expression of different genes in RAW264.7 macrophages for 2D monolayer, 3D single bioprinted and 3D bioprinted RAW264.7/GL261 co-culture model. Data represent mean ± SEM for at least 3 independent experiments. Statistical analysis was performed by two-tailed unpaired student's t-test. *$p < 0.05$, **$p < 0.01$, ***$p < 0.001$.

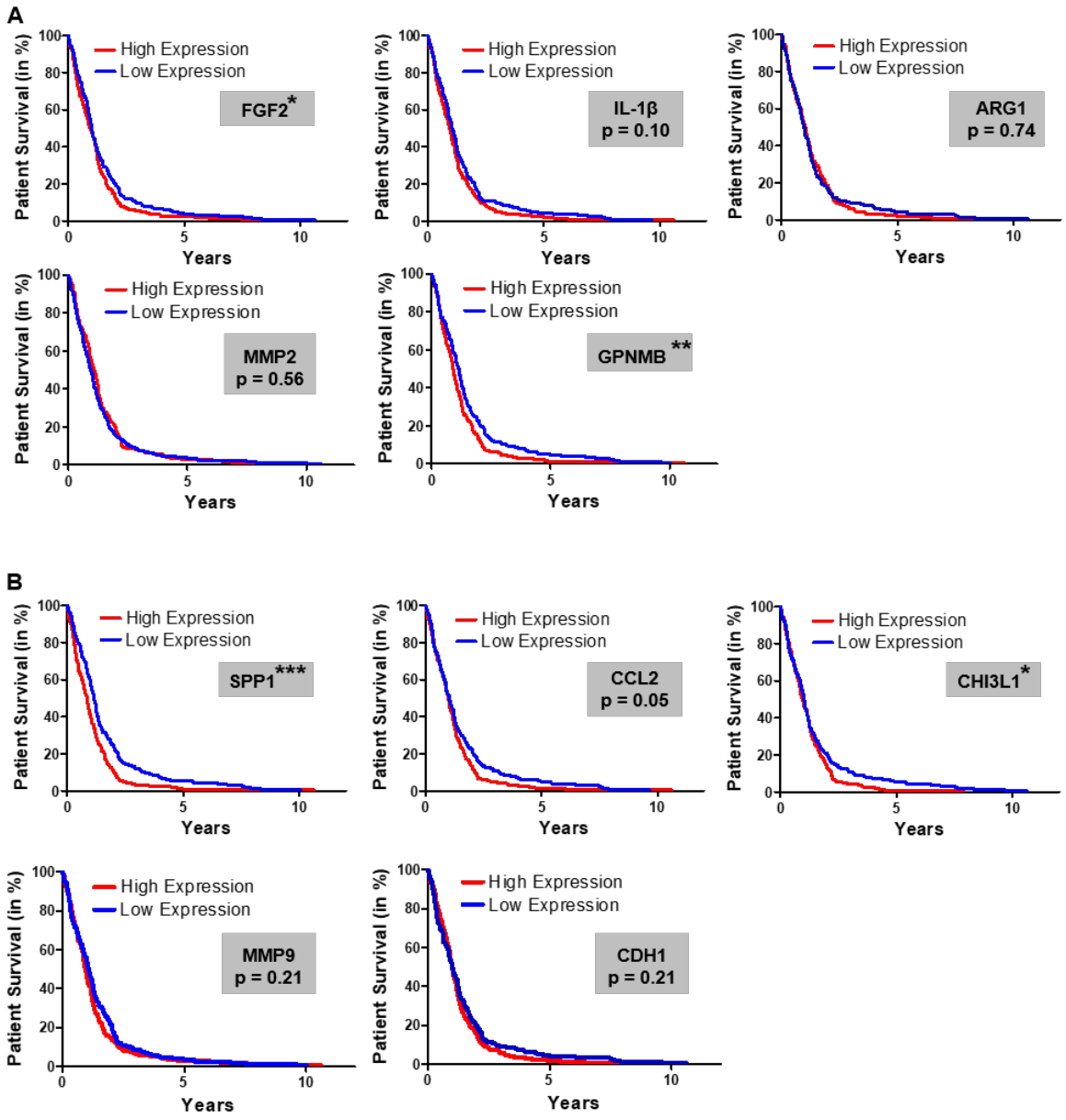

Supplementary Figure S10 Survival of patients (TCGA dataset) for genes displayed in transcriptomic analysis. A, B) Survival analysis of human patients in cohort (TCGA) depending on the high or low expression of genes upregulated (A) primarily for RAW264.7 macrophages and (B) primarily for GL261 glioblastoma cells. Statistical analysis for patient survival was performed by Mantel-Cox test. *$p < 0.05$, **$p < 0.01$, ***$p < 0.001$.

Supplementary Table S1 Gene abbreviations

Abbreviation	Forward Primer (5' > 3')
Fgf2	*Fibroblast Growth factor 2*
Il-1β	*Interleukin 1β*
Arg1	*Arginase 1*
Mmp2	*Matrix metallopeptidase 2*
Ccl2	*C-C motif chemokine ligand 2*
Mrc1	*Mannose receptor C-type 1*
Nos2	*Nitric oxide synthase 2*
Mmp9	*Matrix metallopeptidase 2*
Fgfr1	*Fibroblast growth factor receptor 1*
Spp1	*Secreted phosphoprotein 1*
Il-10	*Interleukin 10*
Il-6	*Interleukin 6*
Ccr2	*C-C motif chemokine receptor 2*
Wnt3a	*Wingless-type MMTV integration site family, member 3A*
Stat6	*Signal transducer and activator of transcription 6*
Wnt5a	*Wingless-type MMTV integration site family, member 3A*
Vim	*Vimentin*
Gpnmb	*Glycoprotein NMB*
Chil1	*Chitinase-like 1*
Gfap	*Glial fibrillary acidic protein*

Olig2	*Oligodendrocyte transcription factor 2*
Pdgfrβ	*Platelet-derived growth factor receptor β*
Timp1	*Tissue inhibitor of metalloproteinase 1*
Map2	*Microtubule-associated protein 2*
Nes	*Nestin*
Cdh1	*Cadherin 1*

Supplementary Table S2 Primers used in real-time PCR for GL261 glioblastoma cells.

Gene	Forward Primer (5' > 3')	Reverse Primer (5' > 3')
Gapdh	*ACAGTCCATGCCATCACTGC*	*GATCCACGACGGACACATTG*
Mmp 2	*TTTCTATGGCTGCCCCAAGG*	*GTCAAGGTCACCTGTCTGGG*
Mmp 9	*TGGGCGTTAGGACAGAAAT*	*GAGTCTGGGGTCTGGTTTCA*
Spp1	*AGCCATGAGTCAAGTCAGCT*	*CCTGGCTCTCTTTGGAATGC*
Ccl 2	*GTGCTGACCCCAAGAAGGAA*	*GTGCTGAAGACCTTAGGGCA*
Gfap	*GAGGGACAACTTTGCACAGG*	*TCCTCCAGCGATTCAACCTT*
Map 2	*TCAGGAGACAGGGAGGAGAA*	*GCAGTTGATCCAGGGGTAGT*
Olig 2	*AGCCCGCTGTTTCTTTCTG*	*CCCACGTTGTAATGCAGGTC*
Chil 1	*CTGAGAGACGCACTGCTTTC*	*TCCAGCCCATCAAAGCCATA*
Gpnmb	*TTCGTGACCATGTCCCAGAA*	*ATGGCAGAGTCGTTGAGGAA*
Fgf 2	*GGCTTCTTCCTGCGCATCCA*	*GCTCTTAGCAGACATTGGAAGA*
Pdgfrβ	*GCTGGAGCTGAGTGAGAGTC*	*GCAGGTAGACCAGGTGACAT*
Fgfr 1	*GCTGACTCCAGTGCATCCAT*	*ACACGGTTGGGTTTGTCCTT*
Timp 1	*ATCAGTGCCTGCAGCTTCTT*	*TGACGGCTCTGGTAGTCCTC*
Nes	*AACAGAGGTGGGAGGATGTG*	*AGTTTCCACTCCTGTAGCCC*
Vim	*TCCAGAGAGAGGAAGCCGAA*	*AAGGTCAAGACGTGCCAGAG*
Cdh 1	*AACCCAAGCACGTATCAGGG*	*GAGTGTTGGGGGCATCATCA*
Wnt3a	*TCCTGTCTGGGATACGGGTT*	*TGTCGGGTCAAGAGAGGAGT*
Wnt5a	*CAAGGAGTTCGTGGACGCTA*	*GCTACAGGAGCCAGACACTC*

Supplementary Table S3 Primers used in real-time PCR for RAW264.7 macrophages.

Gene	Forward Primer (5' > 3')	Reverse Primer (5' > 3')
Gapdh	*ACAGTCCATGCCATCACTGC*	*GATCCACGACGGACACATTG*
Mmp 2	*TTTCTATGGCTGCCCCAAGG*	*GTCAAGGTCACCTGTCTGGG*
Mmp 9	*TGGGCGTTAGGACAGAAAT*	*GAGTCTGGGGTCTGGTTTCA*
Fgf 2	*GGCTTCTTCCTGCGCATCCA*	*GCTCTTAGCAGACATTGGAAGA*
Il-6	*TGATGCTGGTGACAACCACGGC*	*TAAGCCTCCGACTTGTGAAGTGGTA*
Il-1β	*GCCAAGACAGGTCGCTCAGGG*	*CCCCCACACGTTGACAGCTAGG*
Spp 1	*AGCCATGAGTCAAGTCAGCT*	*CCTGGCTCTCTTTGGAATGC*
Il-10	*TGGGTTGCCAAGCCTTATCG*	*TTCAGCTTCTCACCCAGGGA*
Fgfr 1	*GCTGACTCCAGTGCATCCAT*	*ACACGGTTGGGTTTGTCCTT*
Ccl 2	*GTGCTGACCCCAAGAAGGAA*	*GTGCTGAAGACCTTAGGGCA*
Ccr 2	*AGGAGCCATACCTGTAAATGC*	*TGTGGTGAATCCAATGCCCT*
Mrc 1	*TGGATGGATGGGAGCAAAGT*	*GCTGCTGTTATGTCTCTGGC*
Arg 1	*GTGAAGAACCCACGGTCTGT*	*CTGGTTGTCAGGGGAGTGTT*
Nos 2	*GGTGAAGGGACTGAGCTGTT*	*GCTACTCCGTGGAGTGAACAA*
Stat 6	*GTTTACAGTGAAGAAGGCCCG*	*CTGGGCTGGCCCTAAAAACT*
Vim	*TCCAGAGAGAGGAAGCCGAA*	*AAGGTCAAGACGTGCCAGAG*
Wnt3a	*TCCTGTCTGGGATACGGGTT*	*TGTCGGGTCAAGAGAGGAGT*
Wnt5a	*CAAGGAGTTCGTGGACGCTA*	*GCTACAGGAGCCAGACACTC*
Gpnmb	*TTCGTGACCATGTCCCAGAA*	*ATGGCAGAGTCGTTGAGGAA*